

AD



Research and Development Technical Report

ECOM- 0164F

SILICON RF POWER TRANSISTOR METALLIZATION

FINAL REPORT

By

E. HALL

OCTOBER 1971

DISTRIBUTION STATEMENT

Approved for public release;
distribution unlimited.

AD 730774

Reproduced by
NATIONAL TECHNICAL
INFORMATION SERVICE
Springfield, Va. 22151

ECOM

UNITED STATES ARMY ELECTRONICS COMMAND · FORT MONMOUTH, N.J.
CONTRACT DAAB07-70-C-0164

Motorola Inc.
Semiconductor Products Division
Phoenix, Arizona 85008

DDC
RECEIVED
OCT 12 1971
C

DISTRIBUTION STATEMENT A
Approved for public release;
Distribution Unlimited

UNCLASSIFIED

Security Classification

DOCUMENT CONTROL DATA - R & D

Security classification of title, body, of abstract and indexing annotation must be entered when the overall report is classified.

1 ORIGINATING ACTIVITY (Corporate author) Motorola Inc., SPD 5005 E. McDowell Road Phoenix, Arizona 85008		2a. REPORT SECURITY CLASSIFICATION Unclassified	
		2b. GROUP	
3 REPORT TITLE Silicon RF Power Transistor Metallization			
4 DESCRIPTIVE NOTES (Type of report and inclusive dates) Final Report - July 6, 1970 to May 31, 1971			
5 AUTHOR(S) (First name, middle initial, last name) Edward L. Hall			
6 REPORT DATE October 1971		7a. TOTAL NO OF PAGES 97	7b. NO OF REFS 26
8a. CONTRACT OR GRANT NO DAAB07-70-C-0164		9a. ORIGINATOR'S REPORT NUMBER(S) L-58	
b. PROJECT NO IH6 62705A 056			
c. Task No. 01		9b. OTHER REPORT NO(S) (Any other numbers that may be assigned this report) ECOM -0164-F	
d. Subtask 35			
10 DISTRIBUTION STATEMENT Approved for public release; distribution unlimited.			
11 SUPPLEMENTARY NOTES		12 SPONSORING MILITARY ACTIVITY U.S. Army Electronics Command Fort Monmouth, New Jersey 07703 AMSEL-TL-S	
13 ABSTRACT The effects of high temperatures and high current densities on the physical properties of aluminum metallization on semiconductor devices were studied. In particular, this research was concerned with three possible failure modes of the metallization; electromigration, interdiffusion of silicon and aluminum, and metallization reconstruction due to thermal cycling. Electromigration theories are discussed and an engineering curve predicting MTF for an Al-2% Cu alloy was obtained. This alloy has a better MTF than small grained aluminum at all temperatures and is better than large grained aluminum above approximately 70°C. Silicon diffuses into aluminum in a non-uniform manner leaving etch pits whose morphology is determined by the crystallographic orientation of the silicon. Factors governing etch pit location are described. The kinetics of etch pit formation and growth was divided into three stages, i.e., (1) an incubation period related to penetration of any native oxide, (2) the time required to satisfy solubility of silicon in aluminum, and (3) a coarsening process whereby some large etch pits grow at the expense of smaller ones shrinking. Surface reconstruction of aluminum metallization was observed to occur under a wide range of conditions. Even cycling (electrically) between 26°C and 70°C produced roughened metallization after 36,000 cycles in large grained aluminum. The mechanism of this low temperature reconstruction is discussed. Initial reliability studies on two other metallizations, pure tungsten, and gold on PtSi-NiCr-W are also described.			

DD FORM 1 NOV 65 1473

UNCLASSIFIED

Security Classification

14 KEY WORDS	LINK A		LINK B		LINK C	
	ROLE	WT	ROLE	WT	ROLE	WT
Metallization; Metal Migration; Aluminum Swelling						

UNCLASSIFIED

Security Classification

ACCESSION FOR	
CPBT	WHITE S.S.
406	DIFF SEC: <input checked="" type="checkbox"/>
UNANNOUNCED	<input type="checkbox"/>
JUSTIFICATION	<input type="checkbox"/>
BY	
DISTRIBUTION/AVAILABILITY CODES	
DIST.	AVAIL. AND/OR SPECIAL
A	

NOTICES

Disclaimers

The findings in this report are not to be construed as an official Department of the Army position, unless so designated by other authorized documents.

The citation of trade names and names of manufacturers in this report is not to be construed as official Government indorsement or approval of commercial products or services referenced herein.

Disposition

Destroy this report when it is no longer needed. Do not return it to the originator.

TR ECOM-0164F
October 1971

Reports Control Symbol
OSD-1366

SILICON RF POWER TRANSISTOR
METALLIZATION

Final Report
6 July 1970 - 31 May 1971
Contract No. DAAB07-70-C-0164
DA Project No. 1H6 62705A 056

DISTRIBUTION STATEMENT

Approved for public release; distribution unlimited.

Prepared by
E. L. Hall
MOTOROLA INC.

Semiconductor Products Division
5005 East McDowell Road
Phoenix, Arizona 85008

For
U.S. ARMY ELECTRONICS COMMAND, FORT MONMOUTH, N.J.

ABSTRACT

The effects of high temperatures and high current densities on the physical properties of aluminum metallization on semiconductor devices were studied. In particular, this research was concerned with three possible failure modes of the metallization; electromigration, interdiffusion of silicon and aluminum, and metallization reconstruction due to thermal cycling. Electromigration theories are discussed and an engineering curve predicting MTF for an Al-2% Cu alloy was obtained. This alloy has a better MTF than small grained aluminum at all temperatures and is better than large grained aluminum above approximately 70°C. Silicon diffuses into aluminum in a non-uniform manner leaving etch pits whose morphology is determined by the crystallographic orientation of the silicon. Factors governing etch pit location are described. The kinetics of etch pit formation and growth was divided into three stages, i.e., (1) an incubation period related to penetration of any native oxide, (2) the time required to satisfy solubility of silicon in aluminum, and (3) a coarsening process whereby some large etch pits grow at the expense of smaller ones shrinking. Surface reconstruction of aluminum metallization was observed to occur under a wide range of conditions. Even cycling (electrically) between 26°C and 70°C produced roughened metallization after 36,000 cycles in large grained aluminum. The mechanism of this low temperature reconstruction is discussed. Initial reliability studies on two other metallizations, pure tungsten, and gold on PtSi-NiCr-W are also described.

TABLE OF CONTENTS

<u>Section</u>	<u>Title</u>	<u>Page</u>
1.0	INTRODUCTION	1
2.0	ELECTROMIGRATION	4
2.1	Introduction	4
2.2	Electromigration Theories and Comparison to Experiments	4
2.3	Experimental Methods	11
2.4	Electromigration in Aluminum	15
2.5	Electromigration of Aluminum Test Conductors on Silicon	15
2.6	Electromigration in Aluminum Alloys	16
2.7	Electromigration Studies of an Al-2% Cu Alloy Using the Scanning Electron Microscope	23
2.8	Electromigration in Tungsten	34
2.9	Electromigration in Gold	35
2.10	Summary	35
3.0	SOLID STATE DISSOLUTION OF SILICON INTO ALUMINUM	37
3.1	Introduction	37
3.1.1	Previous Work	38
3.2	Qualitative Features of the Silicon Dissolution Process	42
3.2.1	Morphology of the Etch Pits in <111> and <100> Silicon Substrates	43
3.2.2	Location of Etch Pits in Silicon Substrates	49
3.3	Resistivity Increase of Aluminum with Addition of Silicon	55
3.4	Kinetics of the Silicon Dissolution Process	58

TABLE OF CONTENTS (Cont'd.)

<u>Section</u>	<u>Title</u>	<u>Page</u>
3.5	Metallographic Study of the Silicon Dissolution Process	60
3.6	Summary	69
4.0	SURFACE RECONSTRUCTION OF ALUMINUM METALLIZATION DUE TO THERMAL CYCLING	71
4.1	Introduction	71
4.1.1	Previous Work	72
4.2	Experimental Observations	73
4.2.1	High Temperature-Few Cycles (Device Processing)	73
4.2.2	Low Temperature-Many Cycles (Device Operation)	75
4.3	Discussion on Mechanisms for Surface Reconstruction	88
4.3.1	Mechanisms of High Temperature Surface Reconstruction	88
4.3.2	Mechanisms of Low Temperature Surface Reconstruction	89
4.4	Summary	92
5.0	CONCLUSIONS AND RECOMMENDATIONS	94
5.1	Electromigration	94
5.2	Silicon Dissolution	95
5.3	Surface Reconstruction due to Thermal Cycling	96
5.4	Tungsten Metallization	96

LIST OF ILLUSTRATIONS

<u>Figure</u>	<u>Title</u>	<u>Page</u>
1	One Mil Wide Aluminum Test Conductor Stressed at 10^6 amps/cm ² (T = 200°C)	5
2	Schematic of Electrical Arrangement Used in the Electromigration Experiments	5
3	Resistance of a Pure Aluminum Test Conductor as a Function of Temperature	13
4	ΔT of an Aluminum Test Conductor on a TO-5 Header in Air and in Silicone Oil vs $I^2 R_0$	14
5	Median Time to Failure Determination of Aluminum Metallization on Silicon	17
6	Effects of Elements In and Out of Solution on the Resistivity of Aluminum	18
7	Table of Results on Electromigration Tests on Some Aluminum Alloys	20
8	Median Time to Failure of Some Aluminum Alloys as a Function of Current Density j, temperature T, and Cross Sectional area A	21
9	Copper X-Ray Image of the Positive End of a One Mil Wide Al-2% Cu Test Conductor After Electromigration	24
10	SEM Secondary Electron Image Photograph of the Same area of the Al-2% Cu Test Conductor as Shown in Figure 9. (Slightly Smaller Magnification)	24
11	Metallization Test Pattern for Studies Using EBIC Mode of the Scanning Electron Microscope	25
12	Secondary Electron Image of Al-2% Cu Alloy Thin Film Showing Surface Detail (X5000)	27

LIST OF ILLUSTRATIONS (Cont'd.)

<u>Figure</u>	<u>Title</u>	<u>Page</u>
13	Backscatter Electron Image of Al-2% Cu Alloy Thin Film Showing Surface Detail and Some Information of θ Particle Location	27
14	Electron-Beam-Induced Current Image of Al-2% Cu Alloy Thin Film.	27
15	Cross Section of the Top Part of the Test Structure Illustrating the EBIC Mode of the SEM	28
16	EBIC Display of Test Pattern After Electromigration Showing the Migration-Induced Coarsening in the Powered Stripe	30
17	EBIC Display of Negative End of One Mil Wide Test Conductor Before and After Electromigration	31
18	EBIC Display Near the Positive End of the Test Conductor After Electromigration	31
19	A Sequence of EBIC Displays at the (-) End of the Conductor Stripe During the Electromigration Test (Taken Off the T.V. Monitor). Void Growth and Void-Particle Interaction are Evident	32
20	A Sequence of EBIC Displays Taken During the Electromigration Test Showing the Coarsening Process at the (+) End	33
21	Aluminum-Silicon Phase Diagram (From Hansen ⁽¹¹⁾)	39
22	Solubility of Silicon in Aluminum vs Temperature	40

LIST OF ILLUSTRATIONS (Cont'd.)

<u>Figure</u>	<u>Title</u>	<u>Page</u>
23	Chemical Diffusion in Al-Si Alloys	41
24	Scanning Electron Microscope Pictures of an Al-Si Ohmic Contact Before and After Removal of the Aluminum Metallization	44
25	Higher Magnification SEM Picture of Etch Pits in Silicon. SEM Pictures of Replicas (Two Photos on Right) are of the Same Area as the Regular SEM Picture (Left)	45
26	Morphology of an Etch Pit in <100> Silicon	46
27	Morphology of Etch Pits in <111> Silicon	48
28	SEM Picture of Pit in Small Ohmic Contact Area Showing Extension Under Oxide	50
29	Influence of Scratches in the Silicon on Etch Pit Location	52
30	Influence of Aluminum Grain Boundaries on Etch Pit Location	53
31	Influence of High Doping on Etch Pit Shape (Replicas)	54
32	Electromigration Effects on the Silicon Dissolution Process	56
33	Electrical Analog of Ohmic Contact	57
34	Dark Field Optical Micrographs Showing the Number and Size of Etched Pits in <111> Silicon After Three Aging Times (405°C). The Aluminum has been Removed	62
35	The Number of Pits Per Unit Area vs Time for a Sample Aged at 405°C	63

LIST OF ILLUSTRATIONS (Cont'd.)

<u>Figure</u>	<u>Title</u>	<u>Page</u>
36	The Areal Fraction vs Time for a Sample Aged at 405°C	64
37	Diameter of the Largest Pit vs Time for a Sample Aged at 405°C	65
38	Rate of the Reaction $\text{Al} + \text{SiO}_2 \longrightarrow \text{Al}_2\text{O}_3 + \text{Si}$	66
39	Graphic Solution for Concentration of Silicon in an Aluminum Film of Thickness l , Diffusion Coefficient D and Solid Solubility C_∞ , as a Function of Time t	68
40	Scanning Electron Microscope Pictures of a Small Grained (< 1 Micron) Aluminum Thin Film on an Oxidized Silicon Wafer Before and After 10 Cycles for 15 Minutes Duration/Cycle Between 400°C and Room Temperature	74
41	Scanning Electron Microscope Pictures of Medium grained (~ 1-2 Microns Diameter) Aluminum Thin Film on an Oxidized Silicon Wafer Before and After 10 Cycles for 15 Minutes Duration/Cycle Between 400°C and Room Temperature	76
42	SEM Pictures of a Large Grained (~ 8 μm) Aluminum Thin Film on an Oxidized Silicon Wafer Before and After 10 Cycles for 15 Minutes Duration/Cycle Between 400°C and Room Temperature	77
43	SEM Pictures of an Al-2% Cu Thin Film on an Oxidized Silicon Wafer Before and After 10 Cycles for 15 Minutes Duration/Cycle Between 400°C and Room Temperature	78

LIST OF ILLUSTRATIONS (Cont'd.)

<u>Figure</u>	<u>Title</u>	<u>Page</u>
44	Copper X-Ray Images of an Al-2% Cu Thin Film on an Oxidized Silicon Wafer Before and After Aging at 400°C.	79
45	Schematic of Low Temperature-Rapid Cycling Test. The General Pulse Shape is also Shown Indicating the Increase in Voltage Drop as the Stripe Heats Up	81
46	Optical Microscope Photograph of a One Mil Wide Large Grained Aluminum Test Conductor After Low Temperature Thermal Cycling for One Hour ($\Delta T \simeq 70^\circ\text{C}$)	82
47	SEM Pictures of Aluminum Test Conductors With Large Grain Size ($\sim 8 \mu\text{m}$) after Low Temperature ($\Delta T \sim 70^\circ\text{C}$) Thermal Cycling by Electrically Pulsing	83
48	High Magnification SEM Photograph of Thermally Cycled Large Grained Aluminum Showing the Intrusions and Extrusions	84
49	Severe Reconstruction Observed in a Small Grained Aluminum Test Conductor After Pulsing 36,000 times with a $\Delta T \sim 255^\circ\text{C}$	86
50	Metal Reconstruction Observed on a Transistor After Pulsing the Junction 20,000 times, 3 Minutes on and 3 Minutes off, at a Calculated Junction Cycle Temperature of $\Delta T \sim 150^\circ\text{C}$	87
51	Schematic of Fatigue Induced Metal Reconstruction	91

SECTION I

1.0 INTRODUCTION

This report describes work carried out under Contract DAAB07-70-C-0164 from 6 July 1970 to 31 May 1971. The objectives of this research were to study metallization systems used in silicon RF power transistors and to obtain knowledge on the fundamental mechanisms which limit reliability of these devices. In particular, the effects of high temperature and high current densities on the physical properties of the metallization have been studied.

A major effort of this work was directed toward the aluminum metallization system, as this metal is widely used as the contact metallization in silicon power transistors. Operating devices at high temperature and/or high current densities for extended periods of time can cause the metallization of the device to degrade. This research was concerned with three possible failure modes of the aluminum metallization: electromigration; interdiffusion of silicon and aluminum; and metallization reconstruction due to thermal cycling.

High current densities have been shown to cause electromigration of the metal atoms, leaving voids which coalesce and ultimately create an open circuit. This migration of atoms is, among other things, a function of the current density and the diffusivity of the material at the given temperature. The diffusivity of the aluminum atoms depends on the grain size, grain orientation, and amount of impurities, and thus can vary orders of magnitude between various types of aluminum metallization.

A diffusion couple exists when aluminum is in contact with silicon. At any temperature there will be some interdiffusion of aluminum and silicon until solubility requirements are satisfied. The diffusion of aluminum into silicon is negligible at all temperatures of interest in this research. However, the diffusion of silicon into aluminum is not negligible, especially at die bond and wire bond temperatures and in devices which operate at elevated temperatures for extended periods of time. It is found that the silicon diffuses into the aluminum from localized areas in the substrate, creating "etch pits". These etch pits may grow large enough to short out junctions in a power transistor. Silicon dissolution is accelerated when the metallization carries high current densities. Silicon which has diffused into the aluminum is moved "downstream" by electromigration. As the amount of silicon in this region is less than the equilibrium concentration, more silicon from the substrate is able to diffuse into the aluminum. The etch pits grow larger, and regions of high resistivity form in the aluminum where the silicon finally precipitates.

Aluminum metallization has been shown to undergo severe roughening when subjected to thermal cycling. This roughening may lead to device failure by itself or in combination with electromigration since the roughening creates thin regions in the metallization and the current densities will naturally be higher in these regions. The thermal cycling can occur in a device as a result of dissipation of power during pulsed operation.

Electromigration, silicon dissolution, and thermal cycling of the aluminum metallization can all be limiting mechanisms on device reliability. The second part of this research has been to investigate other metallization systems which would be less subject

to the above three failure modes. One very promising approach is the improvement of the aluminum metallization by alloy additions. The alloy, Al-2% Cu, has been studied in detail and is shown to be superior to pure aluminum with respect to electromigration and to surface reconstruction due to thermal cycling. Another approach is to use a different metallization. Pure tungsten appears to be a very promising single metal system and experiments were begun to study the electromigration characteristics of this metal.

In the following sections the work on each of these three possible failure modes is described in detail. Relevant research by other workers has also been included. The aim of this work is to obtain a better understanding of the materials and of the basic mechanisms which cause these materials to degrade. Only after these mechanisms are known and understood can design limits be set.

SECTION II

2.0 ELECTROMIGRATION

2.1 INTRODUCTION

Electromigration is the transport of atoms through a metal or alloy resulting from the passage of direct current. This transport is believed to be caused by a frictional force which exists between the atoms and charge carriers. Because the cross sectional area of metallization on semiconductor devices is so small this atom transport is often important, and it can lead to metallization failure. Figure 1 shows a one mil wide aluminum test conductor on SiO_2 stressed at 10^6 amps/cm² at 200°C. The scanning electron microscope shows that the test stripe, which appeared nearly black optically in certain regions, has a severely roughened surface. Metal atoms have been transported "downstream" from the electron source away from some areas and cluster at other sites, growing well-described crystals or non-descript modules (hillocks). At the same time, vacancies have flowed in the opposite direction. These vacancies coalesce at certain regions creating voids which ultimately lead to an open circuit.

2.2 ELECTROMIGRATION THEORIES AND COMPARISON TO EXPERIMENTS

The total force acting on the atoms (ions) in the metal is composed of two components:

- (1) A force due to the interaction between the electric field, E , and the charge on the positive ion

$$F_i = qE$$

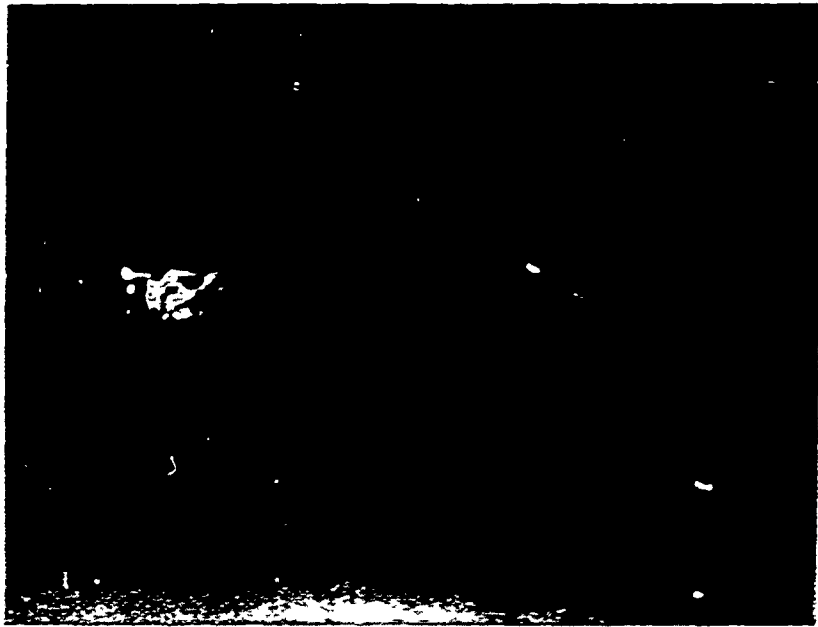


Figure 1. One Mil Wide Aluminum Test Conductor Stressed at 10^6 amps/cm² (T = 200°C)

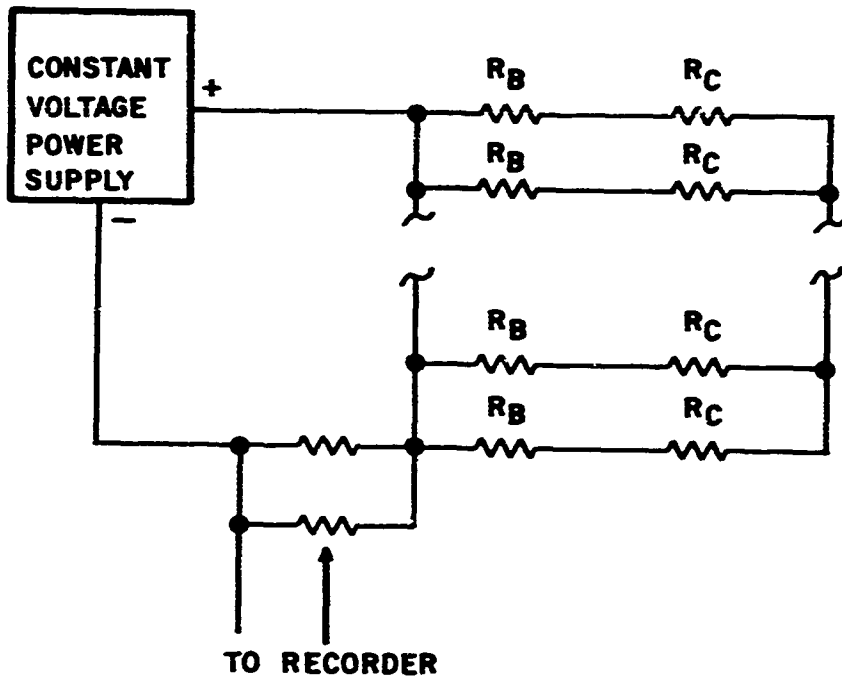


Figure 2. Schematic of Electrical Arrangement Used in the Electromigration Experiments

- (2) A frictional force, F_{ei} , resulting from conduction electrons colliding with the metal atom (ion) and imparting to it additional momentum in the direction of electron flow. Therefore,

$$F = F_i - F_{ei} \quad (1)$$

The exact theoretical description of the F_{ei} force has been a subject of much discussion and is still not resolved. (1, 2) Normally the resulting force in equation (1) is written as

$$F = Z^* qE \quad (2)$$

This force is a function of the position of the metallic ion. When the ion is in a normal lattice site (i.e., completely surrounded by other atoms) the two force components cancel (i.e., $Z^* = 0$), but when the atom is next to a vacancy (or impurity) the atoms scattering cross section is changed yielding a non-zero value for Z^* . Huntington's (3) approximate solution of the force on an atom next to a vacancy in a pure metal results in a value of Z^* of

$$Z^* = 1 - \frac{1}{2} \frac{\Delta\rho}{\rho} \frac{N}{N_d} \frac{m^*}{|m^*|} \quad (3)$$

where $\Delta\rho$ is the extra resistivity that an atom has when next to a vacancy (an activated ion), ρ the specific resistivity of the metal, N is the density of atoms, N_d is the density of such activated

-
- (1) Hehenkamp, Th., "Study of Point Defects in Metals by Electro- and Thermotransport", in Vacancies and Interstitials in Metals, ed. A. Seeger, D. Schumacher, W. Schilling and J. Diehel, Amsterdam, North-Holland, 1969, pg. 91.
- (2) Verhoeven, J., "Electrotransport in Metals", *Met. Rev.* 8 (1963) 311.
- (3) Huntington, H. B. and A. R. Grone, "Current-Induced Marker Motion in Gold Wires", *J. Phys. Chem. Solids* 20 (1961) 76.

ions, and $m^*/|m^*|$, a ratio of the effective masses, gives the sign of the friction force. Z^* , in theory, should depend only on $1/\rho$ as the rest of the terms are nearly constant. However, in practice Z^* has seldom been found to follow this functional dependence.

In any experiment what is observable is not the force itself but the flux of matter, J , (or a result of the flux such as an open circuit) which is produced by the force.

$$J = N\bar{v} \quad (4)$$

The force (F) is related to this flux through the Nernst-Einstein equation for the drift velocity

$$\bar{v} = MF \quad (5)$$

where

- M = mobility = D^*/fkT
- D^* = self-diffusion coefficient = $D_0 e^{-Q/kT}$
- f = a correlation factor which depends on the lattice type
- k = Boltzmann's constant

The ion's drift velocity has been measured by two different methods. In the first method it is calculated from a measured velocity of a scratch inscribed on the surface of the powered conductor (marker motion technique). In the second method a thin layer of material containing a radioactive tracer of the impurity atoms is placed between two halves of a sample. From the concentration distribution after the high current stressing the drift velocity can be

measured directly. Both of the above techniques, at present, have many experimental difficulties.

From equations 2, 4 and 5 and using $E = \rho j$ where j is the current density, the atom flux can be written

$$J = \frac{N D_0 e^{-Q/kT}}{fkT} qZ^* \rho j \quad (6)$$

In the semiconductor industry, to determine the electromigration resistance of a particular metallization, the median time to failure (open) of thin metallic conductors is usually measured. This median time to failure is the time it takes 50 percent of a set of devices to fail under identical operating conditions. The open in the metallization is caused by an accumulation of vacancies at some point in the film, i.e., by a non-vanishing divergence in the atomic flux J . The two main factors resulting in a divergence of the atomic flux are a temperature gradient along the metallization and structural variations (diffusion barriers) in the metallization. Chhabra and Ainslie⁽⁴⁾ showed that if the temperature gradient was a result of Joule heating in the metallization then (from eq. 6)

$$\text{div } J \propto \frac{j^3}{T^3} D_0 e^{-Q/kT} \quad (7)$$

This divergence is proportional to the cube of the current density.

(4) Chhabra, D. S. and N. G. Ainslie, "Open-Circuit Failures in Thin Film Conductors", IBM Technical Report TR22.419.

To obtain the div J due to structural variations they assumed that the divergence was equal to the flux; in other words, that there existed some region in the metallization where vacancies are always trapped and do not proceed further. From equation 6 they obtained

$$\text{div J} \propto \frac{j}{T} D_0 e^{-Q/kT} \quad (8)$$

This divergence is proportional to the current density. The actual structural variations causing this divergence are still being investigated. Grain size variations, grain orientation variations, and compositional variations have all been suggested.

There is no obvious relation between MTF and flux divergence. As a first approximation it will be assumed that

$$\text{MTF} \propto 1/\text{div J} \quad (9)$$

that is, the larger the rate of accumulation of voids the shorter the MTF. Black⁽⁵⁾ showed that MTF is also proportional to the cross sectional area of the conductor. Thus

$$\text{MTF} \propto \frac{A}{\text{div J}} \quad (10)$$

or using equation 8 and assuming no temperature gradient (as is the case in most experiments)

(5) Black, J. R., "Metallization Failures in Integrated Circuits", Tech. Report No. RADC-TR-68-243 Rome Air Development Center, Air Force Systems Command, Griffiss Air Force Base, New York, October 1968.

$$j(\text{MTF}) = \frac{KAT}{D_0 e^{-Q/KT}} \quad (11)$$

where K is a constant. A plot of $\log_{10} \frac{AT}{j(\text{MTF})}$ vs $1/T$ should then yield a straight line with a slope equal to $(-Q/k) \log_{10} e$.

To obtain a better median time to failure for a particular metallization it is thus necessary to increase the cross sectional area or reduce the flux divergence. $\text{div } J$ may be reduced most easily by reducing j , D_0 , or by increasing the activation energy Q .

The above theory predicts a j^1 dependence of current density times MTF. However, the experimental data of Black⁽⁵⁾ and recently d'Heurle⁽⁶⁾ indicate a power between 2 and 3 for current density. This different dependence may be because of temperature gradients due to Joule heating, or in the way MTF is related to the divergence of the flux. Their data, when plotted using j^1 , still yield straight lines with nearly the same activation energies as before, and extrapolation of high temperature results to low temperatures produce only minimal changes in the predicted MTF. However, because of the experimental indication of a j^2 - j^3 dependence, the electromigration results obtained in this work will be compared to previous work⁽⁵⁾ using a j^2 dependence, i.e. $\log [A/j^2(\text{MTF})]$ plotted vs $1/T$.

From the above discussion it is evident that great care must be taken in interpreting electromigration experiments.

(6) d'Heurle, F. M., "The Effect of Copper Additions on Electromigration in Aluminum Thin Films", Met. Trans. 2 (1971) 683.

Many undesirable effects may act on the measured MTF and lead to an incorrect interpretation of the mechanisms involved.

2.3 EXPERIMENTAL METHODS

Units were powered in a constant temperature oven or in a temperature controlled oil bath to obtain the MTF for a particular metallization. Figure 2 is a schematic of the electrical arrangement. A constant voltage was applied across the group of parallel sockets to give the required current through the test conductors. Ballast resistors, R_B , were connected in series to each device to insure that a change in resistance, R_C , of the test conductor would not change the current. The group of devices was monitored continuously with a chart recorder. The percent failed was plotted vs time on distribution graph paper to obtain a median time to failure (50 percent failure).

As indicated in the previous section, accelerating electromigration tests can cause many problems. A major problem is that of Joule heating which not only may introduce temperature gradients but will also increase the temperature of the test conductor. For a wire carrying a current there is a temperature distribution along the wire. This distribution may be calculated theoretically if the heat sinking efficiencies of the header and bonding pads are known. In this work it will be assumed that the test conductor is at uniform temperature. Then the only effect of Joule heating will be to increase the conductor temperature. In general the increase in temperature can be written

$$\Delta T = \theta(I^2R) \quad (12)$$

where θ is a thermal resistance.

Also, for a test conductor at a uniform temperature

$$\frac{R-R_0}{R_0} = a(T-T_0) \quad (13)$$

where R_0 is the resistance at T_0 , R is the resistance at T , and "a" is the temperature coefficient of resistivity

$$\rho = \rho_0 (1 + a \Delta T) \quad (14)$$

Combining equations 12 and 13 to eliminate R yields

$$T-T_0 = \Delta T = \frac{\theta I^2 R_0}{1 - \theta I^2 R_0 a} \quad (15)$$

This equation was used to determine the ΔT due to Joule heating in the electromigration experiments. To check the validity of this equation, the resistance of a one mil wide by 12,000 Å thick by 54 mil long pure aluminum test conductor was measured as a function of temperature to experimentally determine "a" in equation 13, (Figure 3). Then this same test conductor was powered at various high currents to cause Joule heating and the resistance was obtained from the measured voltage drop at each current. ΔT was then calculated from equation 13 and plotted vs $I^2 R_0$ shown in Figure 4. Also plotted is the curve calculated using $\theta = 200^\circ\text{C}/\text{watt}$ (7) and $a = \frac{\Delta\rho/\Delta T}{\rho_0} = \frac{\alpha}{\rho_0} = 4.25 \times 10^{-3}$ where $\rho_0 = 2.71 \mu\Omega\text{cm}$ at 26°C and $\alpha = 0.0115 \mu\Omega\text{cm}/^\circ\text{C}$ (8). The agreement between the experimental and calculated curves is very good. This curve illustrates

- (7) Daniels, R. G., "Heat Transfer and Integrated Circuits", Electro-Technology, January 1969, pg. 22.
- (8) Aluminum, Vol. I, "Properties, Physical Metallurgy, and Phase Diagrams", ed. K. R. VanHorn, American Society for Metals, Metals Park, Ohio, 1967, p. 174-175.

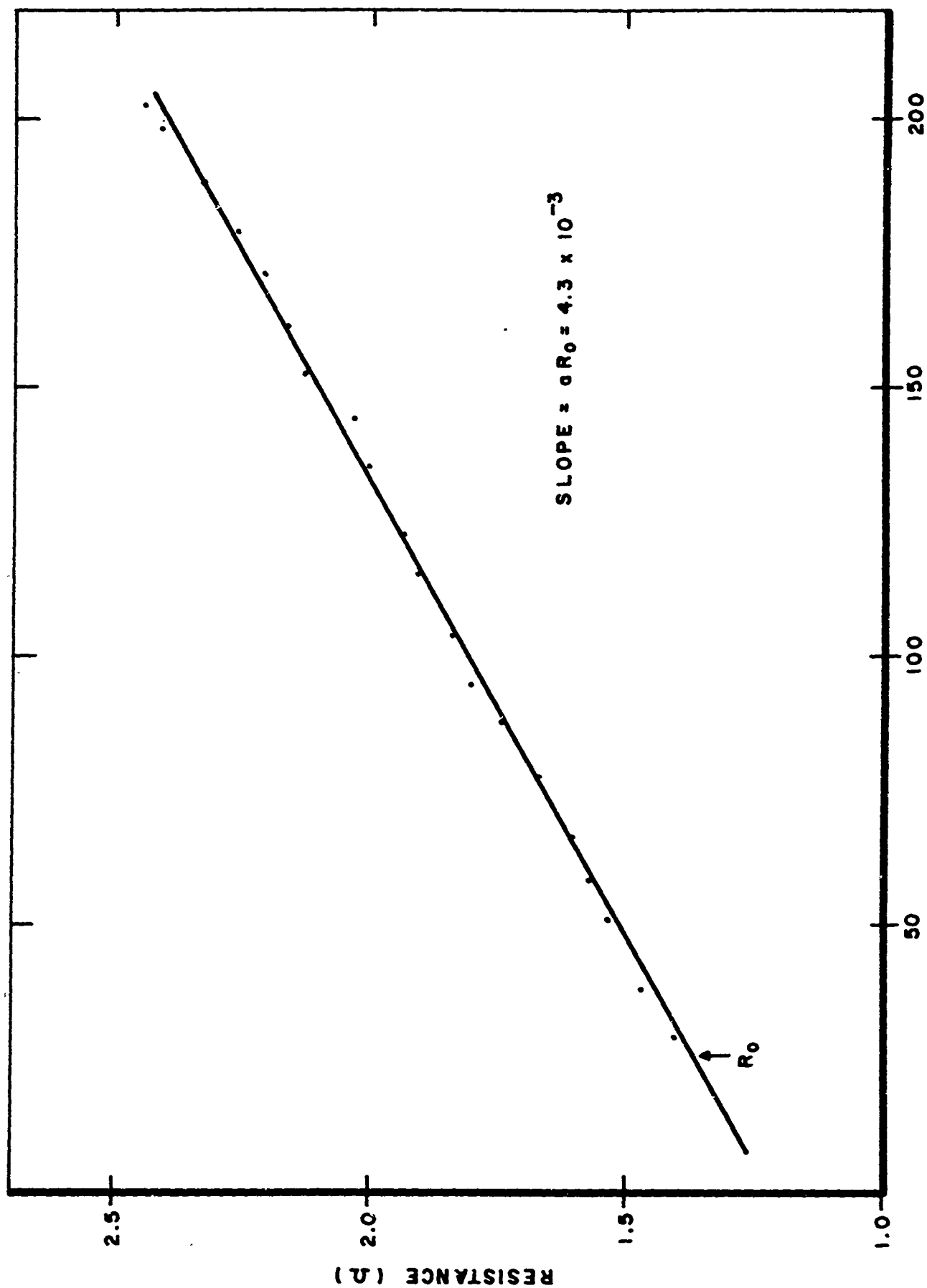


Figure 3. Resistance of a Pure Aluminum Test Conductor as a Function of Temperature

9595-7-1

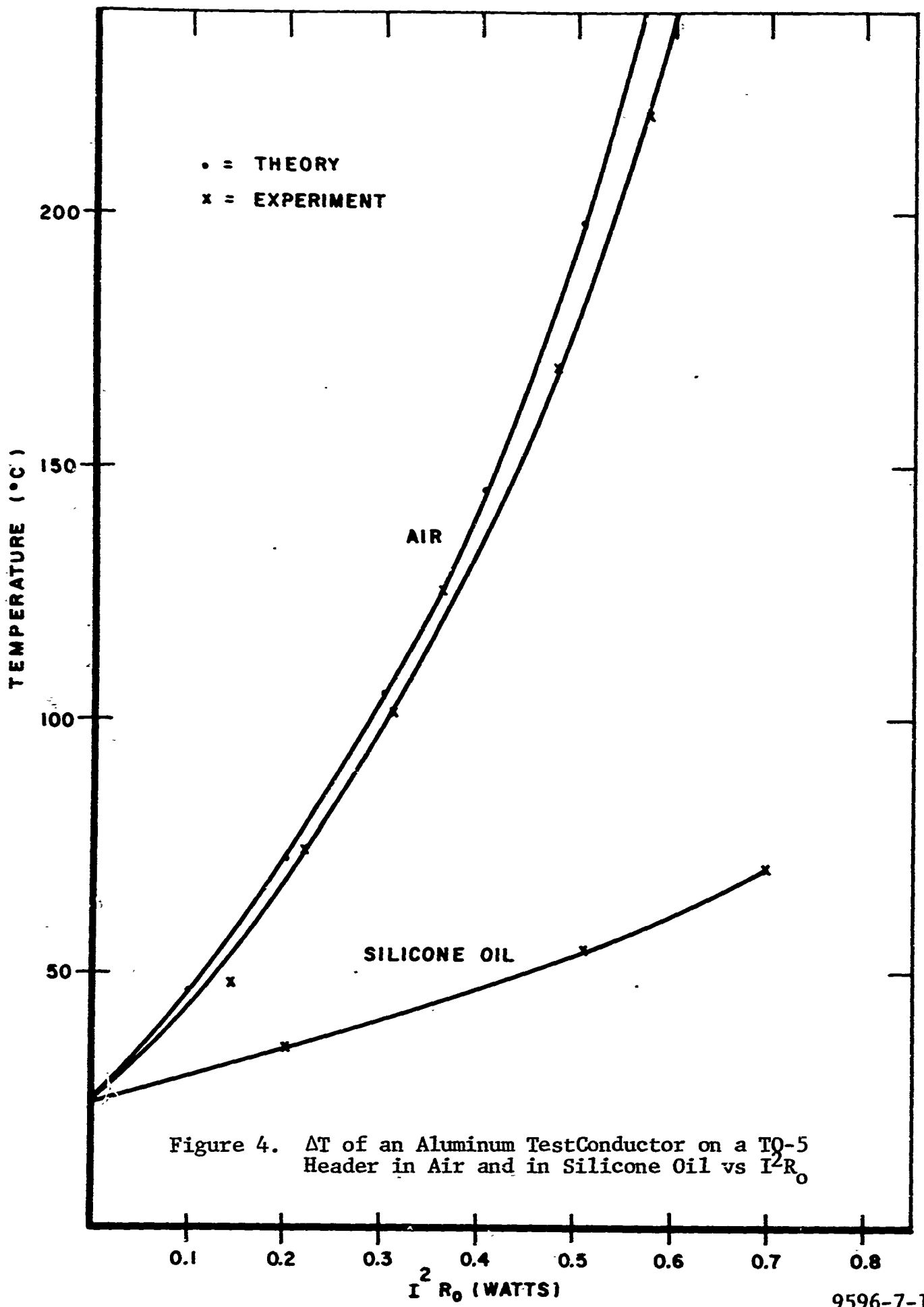


Figure 4. ΔT of an Aluminum Test Conductor on a T0-5 Header in Air and in Silicone Oil vs $I^2 R_0$

the very rapid rise in temperature of the stripe with $I^2 R_0$. Also, from equation 15 it is apparent that there are three factors which determine the increase in temperature due to Joule heating: the heat sinking efficiency, θ , the initial resistance, R_0 , and the coefficient of resistivity, α . The experimentally measured ΔT vs $I^2 R_0$ curve for a test conductor on a TO-5 header in a silicone oil bath is also shown in Figure 4. The oil reduces the ΔT appreciably by lowering θ , allowing higher current densities to be used in the accelerated electromigration experiments with smaller effects due to Joule heating.

2.4 ELECTROMIGRATION IN ALUMINUM

J. Black⁽⁵⁾ has obtained extensive experimental data on the MTF of aluminum test conductors due to electromigration. He has also demonstrated the effect of grain size on MTF. For large-grained material the activation energy Q is nearly that of bulk diffusion in aluminum (1.4eV), while for small-grained aluminum, the activation energy is more nearly that for surface and grain boundary diffusion (0.4-0.6eV). It is possible to compare the electromigration resistance of new metallizations with that of pure aluminum using his curves.

2.5 ELECTROMIGRATION OF ALUMINUM TEST CONDUCTORS ON SILICON

A study was made to see if Black's results were altered when the conductors were in contact with pure silicon instead of SiO_2 . Pure aluminum was deposited at 10^{-8} Torr directly onto a cold (maximum temperature = 75°C) $\langle 100 \rangle$ 30 ohm-cm p-type silicon wafer and patterned in test conductors. Ten devices of cross sectional area $14.2 \times 10^{-8} \text{ cm}^2$ were stressed at $8.9 \times 10^5 \text{ amps/cm}^2$

at a temperature of 196°C. Figure 5 presents a plot on distribution graph paper of percent failed vs hours, yielding a MTF of 100 hours. The MTF predicted from Black's curves at 196°C for un-glassed fine-grained aluminum is 95 hours. Thus, Black's data of pure aluminum on SiO₂ predicts well the MTF of pure aluminum on silicon. One would expect that the silicon dissolution into the aluminum would change the vacancy migration kinetics or the grain boundary diffusion of aluminum. However, this run indicates that these effects are not appreciable in determining the MTF due to electromigration of pure aluminum deposited on silicon. RF power devices have this geometry in their emitter and base contact areas. Note, however, that this geometry is not the same as co-depositing aluminum and silicon to form a binary alloy. In that case, the MTF may be different.

2.6 ELECTROMIGRATION IN ALUMINUM ALLOYS

One promising way of improving the electromigration resistance of aluminum metallization is through the addition of alloying elements. IBM^(9, 6) was the first to show that copper additions to aluminum improved the MTF and their tests indicate that an Al-4% Cu metallization has a MTF at 175°C equivalent to that measured for pure large-grained glassed aluminum. They also reported that additions of Ag and Au did not improve the MTF.

The resistivity of aluminum increases rapidly with most alloying elements. (Figure 6). However, by using small percentages the resistivity can be kept within reasonable limits (below 6 $\mu\Omega\text{cm}$).

(9) Ames, I., F. M. d'Heurle, R. E. Horstmann, "Reduction of Electromigration in Aluminum Films by Copper Doping", IBM, J. Res. Develop. 14 (1970) 461.

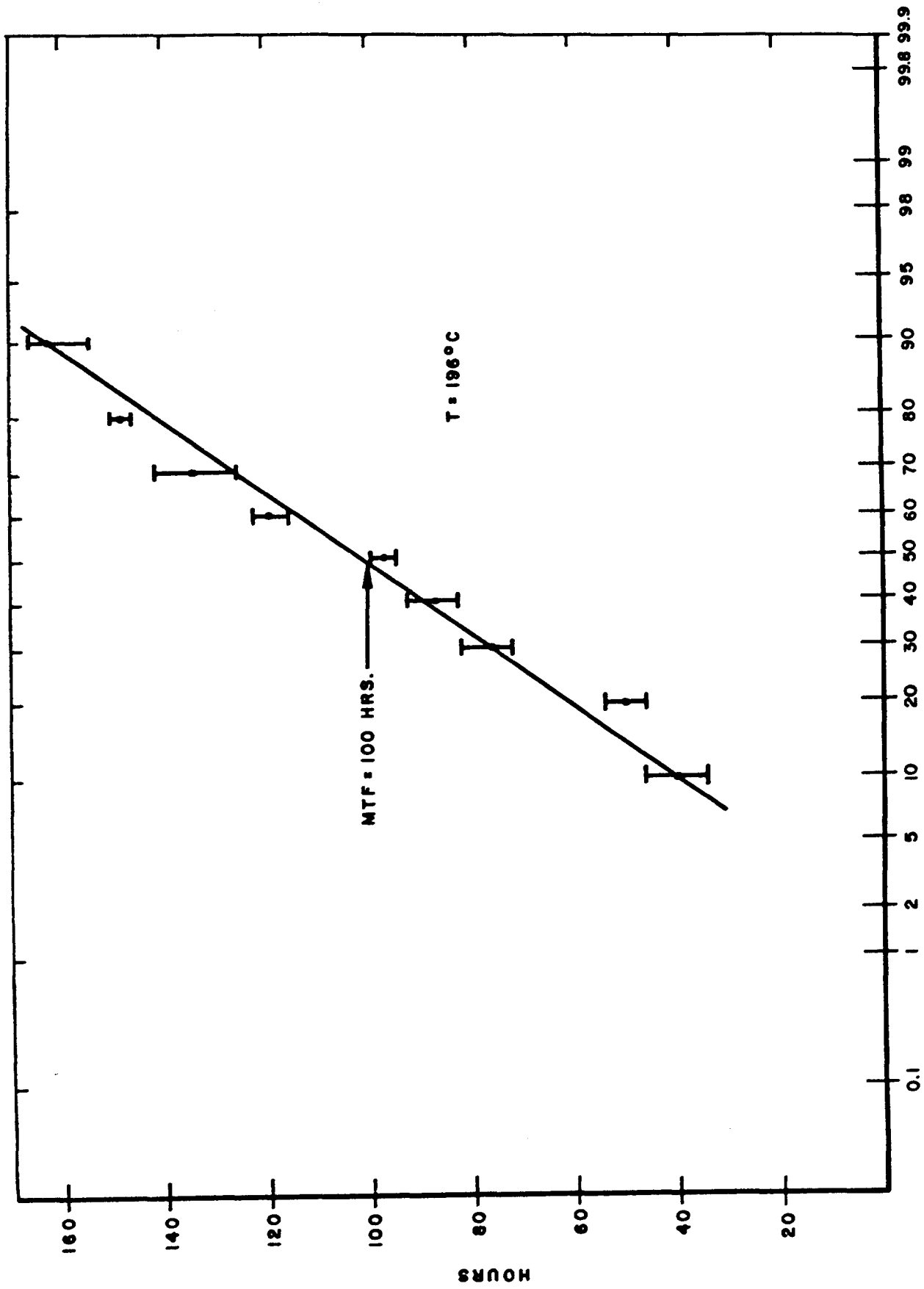


Figure 5. Median Time to Failure Determination of Aluminum Metallization on Silicon

8858a-0-0

<u>Element</u>	<u>Maximum Solubility In Al %</u>	<u>Increase in Resistivity Per WT % Added (Micron m-cm)</u>	
		<u>In Solution</u>	<u>Out of Solution</u>
Cr	.77	4.0	.18
Cu	5.65	.344	.03
Fe	.052	2.56	.058
Mn	1.82	2.94	.34
Ni	.05	.81	.061
Si	1.65	1.02	.088

Figure 6. Effects of Elements In and Out of Solution on the Resistivity of Aluminum

In the following paragraphs in this section electromigration data is presented and discussed for an Al-0.75% Mn alloy, Al-0.45% Fe alloy and an Al-2% Cu alloy. The results are tabulated in Figure 7 and plotted in Figure 8 with the curves obtained by Black for pure aluminum.

Al-0.75% Mn

The units were powered at a current density of $j = 1.2 \times 10^6$ amps/cm² in an oven set at 196°C. From a measured $\rho_0 = 5.4 \mu\Omega\text{cm}$, $R_0 \approx 1$ ohm and assuming $\Delta\rho = 0.0115 \mu\Omega\text{cm}$ and $\theta = 200^\circ$, a $\Delta T = 15^\circ$ due to I^2R heating was calculated from equation 15 giving an operating temperature of 211°C. A MTF of 73 hours was obtained, and plotting this in Figure 8 shows that the addition of manganese has done little to increase the lifetime of aluminum metallization. A microprobe analysis indicated that the manganese concentration was still uniform along the test conductor after electromigration and equal to the concentration in the unpowered region even though many large hillocks had formed. Thus the manganese atoms were not influenced by the electron wind.

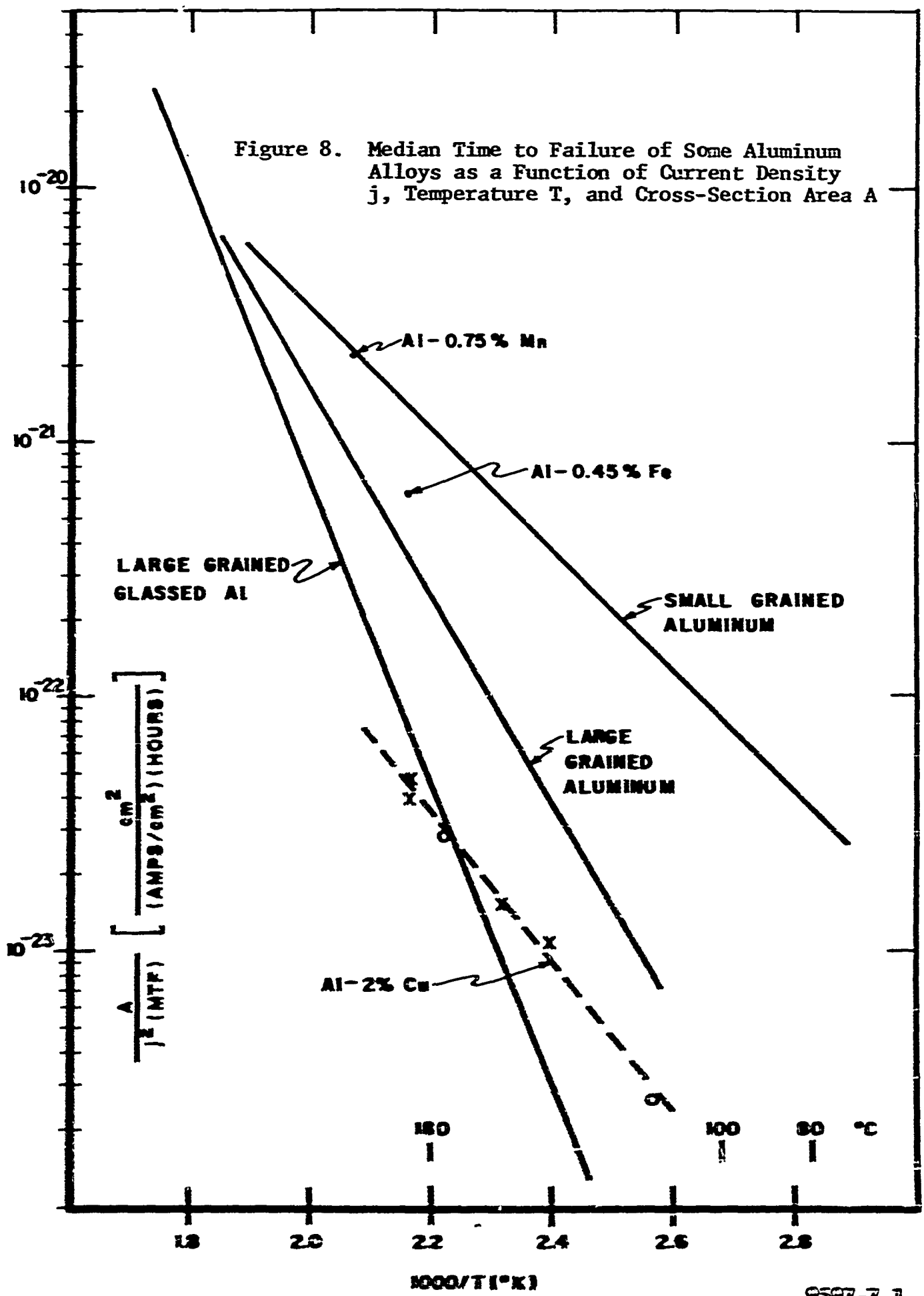
Al-0.45% Fe

The units were powered at $j = 8.4 \times 10^5$ amp/cm² and at a temperature of 190°C (187°C oven temperature plus 3°C due to I^2R heating). The MTF of 360 hours was 2.2 times better than that predicted for small-grained Al test conductors (Figure 8). Because of the small amount of iron in this alloy, it was difficult to determine with the microprobe whether iron atoms had moved. However, appreciably more iron was found just to one side of the break in the stripe, indicating Fe is more mobile than Mn.

	<u>TEMPERATURE</u>	<u>CURRENT DENSITY</u> (amps/cm ²)	<u>CROSS-SECTIONAL AREA</u> cm ²	<u>MTF</u> (hours)
Al-0.75% Mn	211°C	1.2 x 10 ⁶	23.6 x 10 ⁻⁸	73
Al-0.45% Fe	190°C	8.4 x 10 ⁵	16.0 x 10 ⁻⁸	360
Al-2% Cu	145°C	4.0 x 10 ⁶	5.36 x 10 ⁻⁸	315
Al-2% Cu	157°C	3.0 x 10 ⁶	5.36 x 10 ⁻⁸	400
Al-2% Cu	183°C	3.0 x 10 ⁶	5.36 x 10 ⁻⁸	150
Al-2% Cu	183°C	3.0 x 10 ⁶	5.36 x 10 ⁻⁸	140

Figure 7. Table of Results on Electromigration Tests on Same Aluminum Alloys

Figure 8. Median Time to Failure of Some Aluminum Alloys as a Function of Current Density j , Temperature T , and Cross-Section Area A



Al-2% Cu

This alloy was studied in some detail. An engineering curve was obtained to allow MTF predictions at lower temperatures than those used in the accelerated testing. This alloy was also studied using the secondary, backscatter, and electron beam induced current modes of the scanning electron microscope to obtain a better understanding of the beneficial behavior of copper.

Initially electromigration tests were done in ovens using 0.7 mil wide stripes. However, the lifetimes were too long to obtain MTF data in a reasonable length of time. Test conductors with 0.3 mil widths were patterned on only 1000 Å of SiO₂ in order to accelerate the testing and yet keep the Joule heating at a minimum. The experiments were done in temperature controlled silicone oil baths to further decrease the Joule heating and temperature gradients. The ΔT due to Joule heating was obtained experimentally using the curve of Figure 4. Figure 7 gives the results of four runs using the oil bath. These results have also been plotted as x's in Figure 8 along with two points on an Al-2% Cu alloy reported by IBM (O's). These data lie on a line with an activation energy of about 0.6 eV. The measurements indicate the Al-Cu alloy has greater electromigration resistance than "small grained" aluminum at all temperatures and is better than large grained aluminum above approximately 70°C. Above 175°C it is better than "large grained" glassed aluminum. It should be pointed out that the terms "large grained" and "small grained" are relative to the size of the conductor stripe. When the aluminum grain size becomes larger than the stripe width, the predicted MTF should be made using the large grained curves, as grain boundary diffusion has been reduced. The Al-Cu MTF data is probably independent of stripe width since its grain size was extremely small.

Because of its composition and prior heat treatment the Al-2% Cu film consisted of CuAl_2 particles (θ phase) in an aluminum matrix. A microprobe study of the film showed that initially the θ phase distribution was fairly random. At the end of the test a Cu x-ray image indicated a lower than average copper concentration at the negative end. Near the positive end the Cu x-ray image showed several localized regions of very high copper concentration (Figure 9). These regions are seen to be near or below the hillocks observed in SEM secondary electron image photograph (Figure 10). As the Al x-ray image showed almost no signal increase in these areas we can conclude that these areas are much richer in copper. Thus copper is moving in the direction of the electron wind depleting the negative end, while further down the stripe localized regions of high copper concentration are formed. These observations are also confirmed in the next section.

2.7 ELECTROMIGRATION STUDIES OF AN AL-2% Cu ALLOY USING THE SCANNING ELECTRON MICROSCOPE

An Al-2% Cu metallization test conductor deposited onto a specially designed silicon transistor was powered in the scanning electron microscope in order to obtain a better understanding of the beneficial behavior of alloy additions to aluminum. The results of this experiment are described in the following paragraphs.

The special metal test pattern on a large area transistor is shown in Figure 11. The surface metal pattern contains conductors in contact with silicon and SiO_2 areas in addition to the normal transistor contacts. With the device in the SEM, electrons from the electron gun are both transmitted through the metal film and reflected (backscatter and secondary electrons) from its surface.

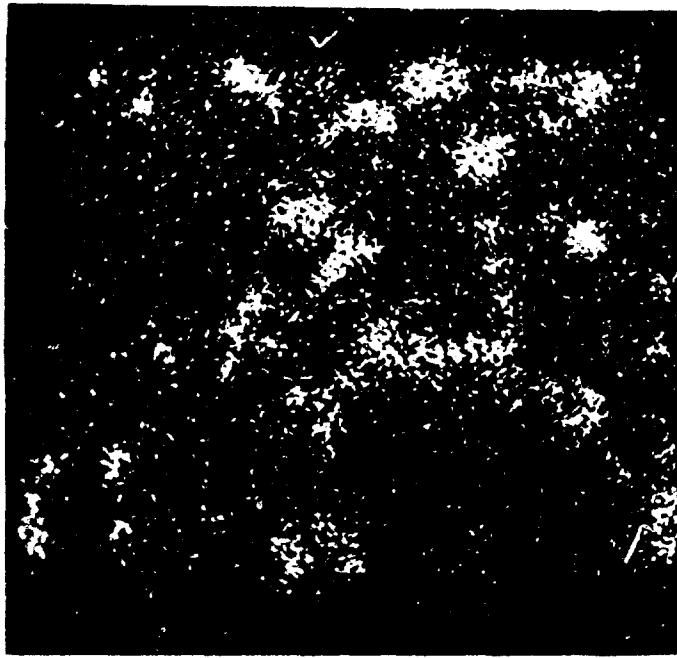


Figure 9. Copper X-ray Image of the Positive End of a One Mil Wide Al-2% Cu Test Conductor After Electromigration

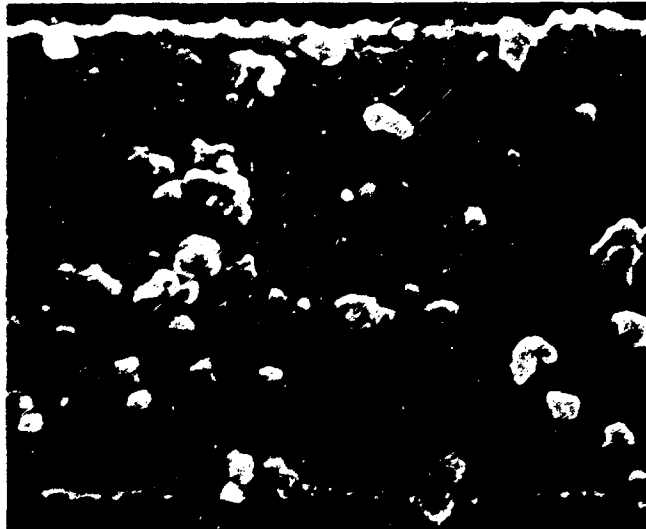


Figure 10. SEM Secondary Electron Image Photograph of the Same Area of the Al-2% Cu Test Conductor as Shown in Figure 9. (Slightly Smaller Magnification)

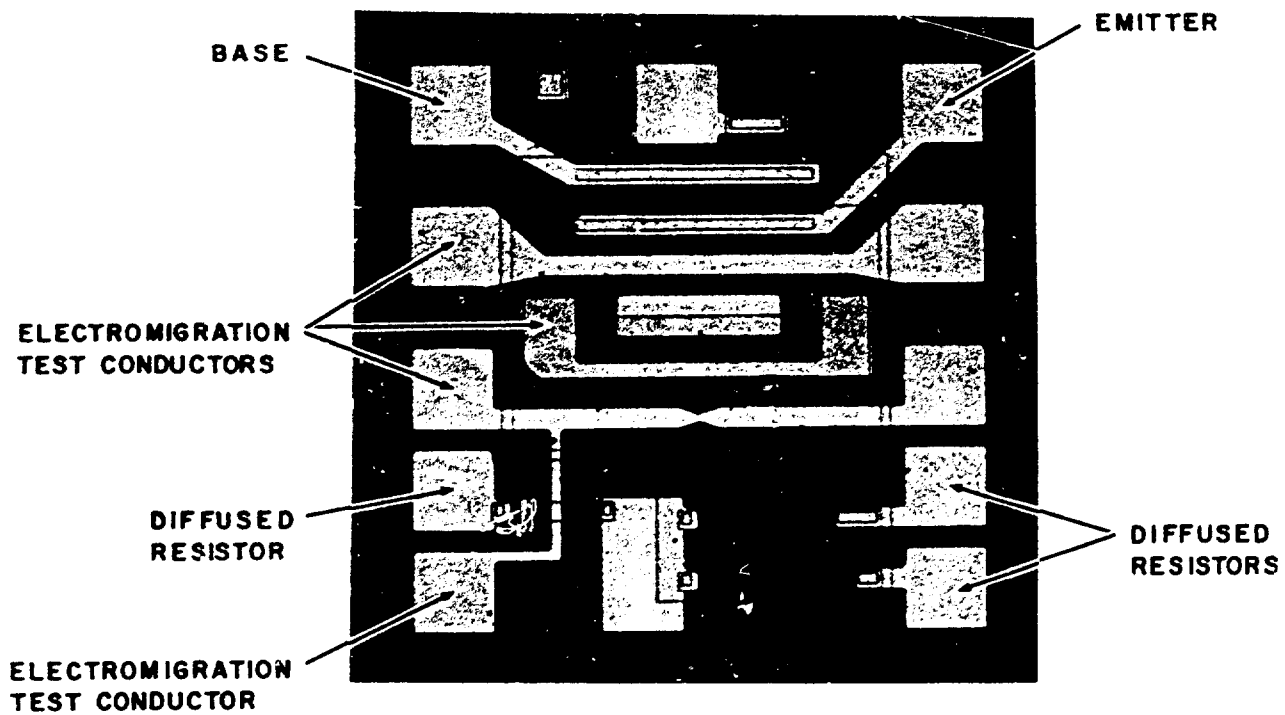


Figure 11. Metallization Test Pattern for Studies Using EBIC Mode of the Scanning Electron Microscope

The secondary electron image is obtained by using a low energy beam (10 kV) and it contains information concerning the metal surface. Using 25 kV electrons produces primarily a backscattered electron image. The intensity of backscattered electrons is a function of the composition and density of the material and it provides both surface and near surface information. Figures 12 and 13 are high magnification SEM pictures in the secondary and backscatter modes of an Al-2% Cu metallization film. The surface information available in Figure 12 becomes lost in the backscatter picture. However, regions of higher density (high Cu concentrations) appear as bright spots because of their greater scattering.

A portion of the electron beam is transmitted through the metal film (Figure 15) into the silicon and there creates one hole electron pair per 3.6 electron volts of energy. These beam generated carriers diffuse and drift to the p-n junction where they can be collected. The amplitude of this electron beam induced current (EBIC) at any one point is a function of the topography and of the mass density of the film. A picture of the same area as Figures 12 and 13, using the EBIC mode, is shown in Figure 14. Because of their higher absorption, the Cu rich areas appear dark compared to the aluminum matrix. In this mode particles throughout the thickness of the film are seen, not just those at the surface or near surface. In fact, stereo EBIC pictures have been made of the Al-Cu alloy. These pictures give a three dimensional view of the Cu rich particles throughout the film.

These three information modes of the SEM -- EBIC, secondary and backscatter -- have been combined with Motorola's rapid scan facility to study the details of electromigration in the Al-Cu alloys while powering in the SEM. As the test proceeded, the θ

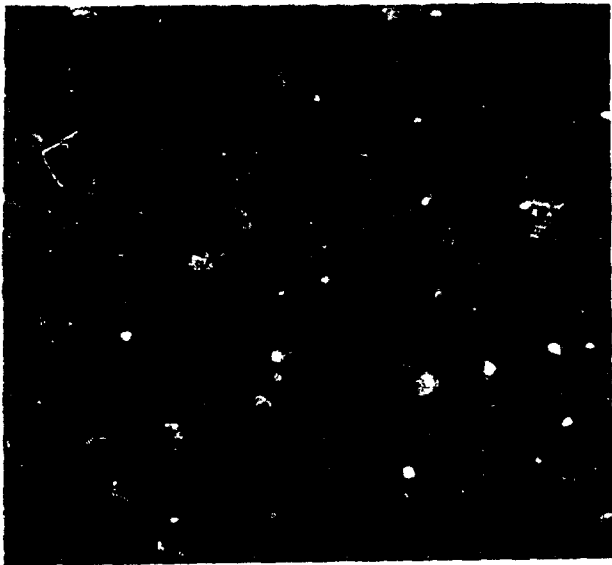


Figure 12. Secondary Electron Image of Al-2% Cu Alloy Thin Film Showing Surface Detail (X5000)

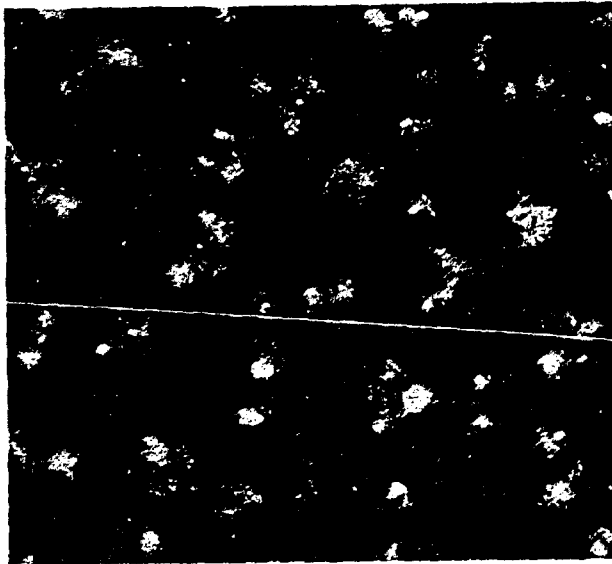


Figure 13. Backscatter Electron Image of Al-2% Cu Alloy Thin Film Showing Surface Detail and Some Information of θ Particle Location (White Areas) (X5000)



Figure 14. Electron-Beam-Induced Current Image of Al-2% Cu Alloy Thin Film. The θ Particles Now Appear Dark. (X5000)

9224-2-1

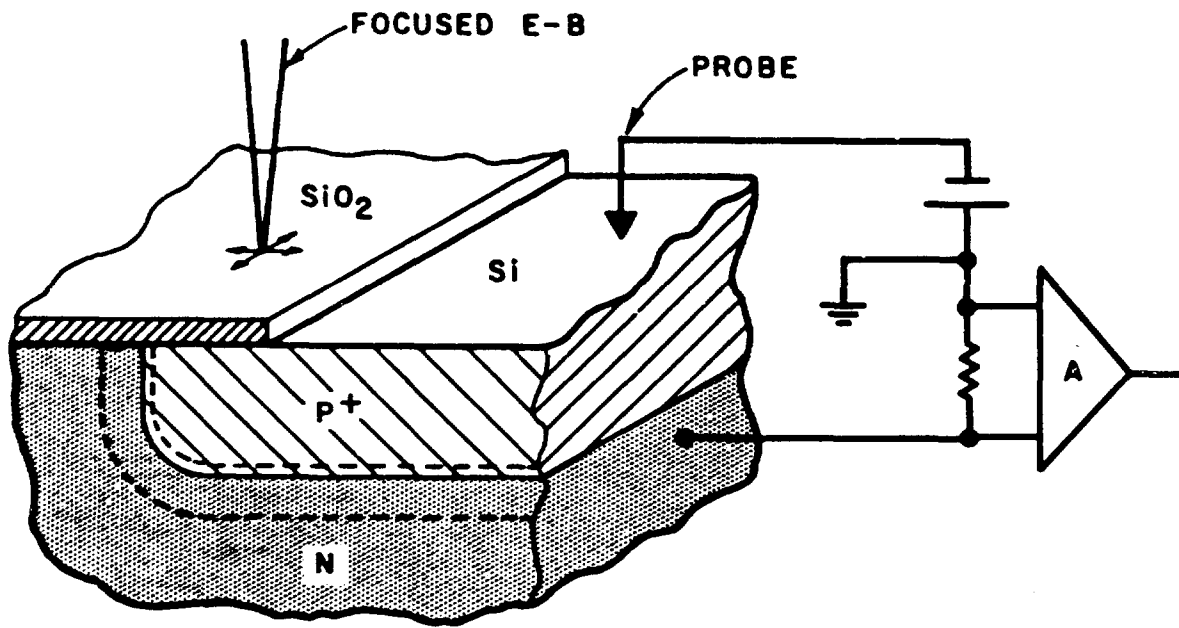


Figure 15. Cross-Section of the Top Part of the Test Structure Illustrating the EBIC Mode of the SEM

phase particles exhibited a migration induced coarsening. Most of the copper disappeared from the negative end and large θ particles grew further down the test conductor and near the positive end. These appeared as hillocks in the secondary electron mode. Only after much of this coarsening had taken place did any voids appear in the metallization. These voids nucleated in regions depleted of copper, moved slowly, and were easily tied to a CuAl_2 particle. Hillocks formed along the conductor and also seemed to be associated with CuAl_2 particles. The stripe finally failed at the negative end after substantial voiding had reduced the cross sectional area at this point. Figure 16 is an EBIC display of the test pattern after the experiment showing the migration induced coarsening as well as the random voiding in the powered stripe. High magnification pictures of the positive and negative ends are shown in Figures 17 and 18. Figure 19 is a sequence of pictures taken off the T.V. monitor, showing void growth and void-particle interaction in the later stages of the experiment. The coarsening process is shown in Figure 20. A motion picture was made of electromigration in Al-2% Cu alloy using the above modes of the SEM.

Thus copper, as does aluminum, migrates in the direction of the electron wind. This movement occurs by the disappearance of certain θ particles and the growth of others further down the metallization. As no large voids became visible until much of this migration has occurred, it is believed that θ particles are sinks for vacancies. Because of the large number of θ particles, only relatively few vacancies become tied to any one particular particle. Only after the depletion of θ particles will the vacancy clusters coalesce and grow into a visible void. In pure aluminum, the lack of all these sinks results in a few large voids which are also fairly mobile. Thus, the Al-Cu alloys

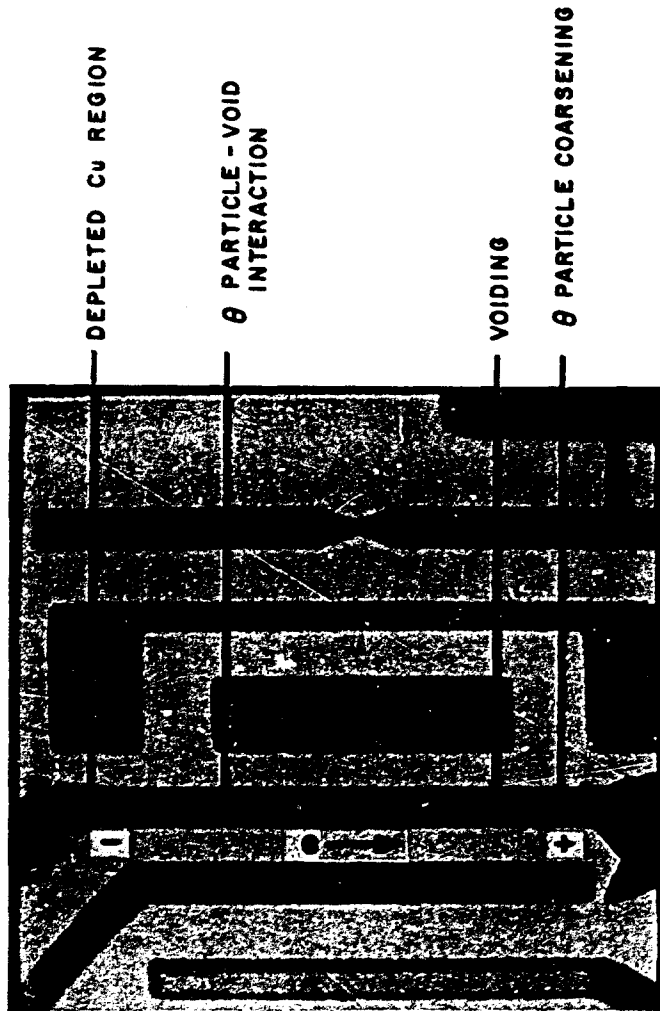
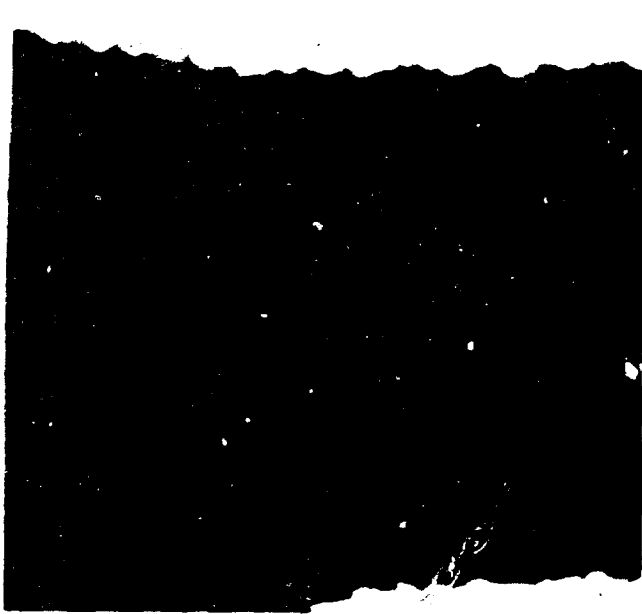


Figure 16. EBIC Display of Test Pattern After Electromigration Showing the Migration-Induced Coarsening in the Powered Stripe



(Before)



(After)

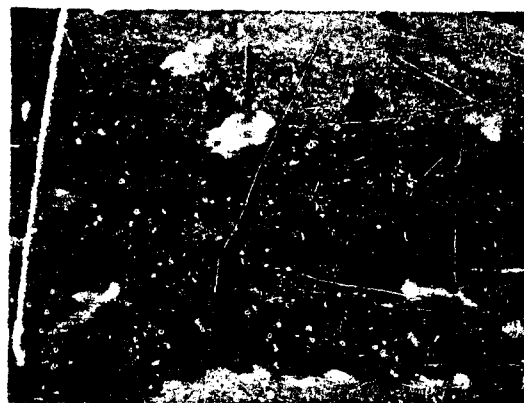
Figure 17. EBIC Display of Negative End of One Mil Wide Test Conductor Before and After Electromigration



Figure 18. EBIC Display Near the Positive End of the Test Conductor After Electromigration



(1)



(2)

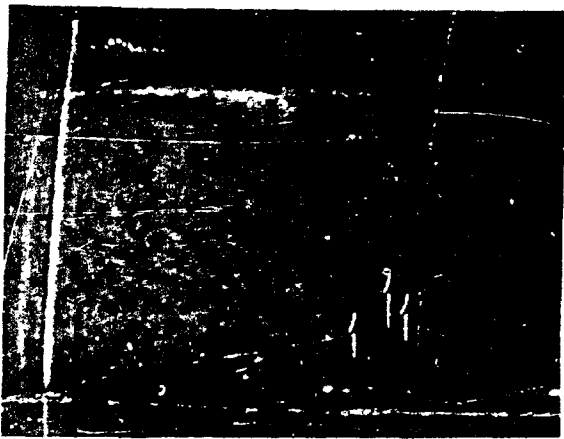


(3)

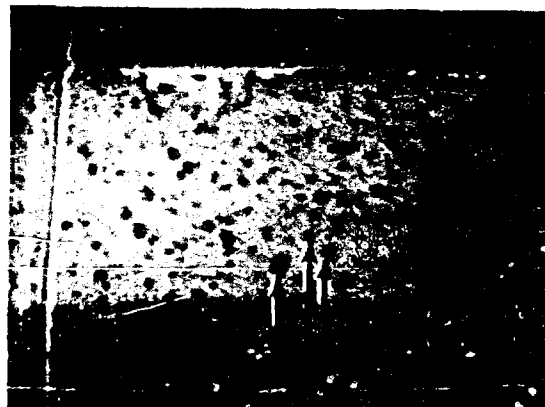


(4)

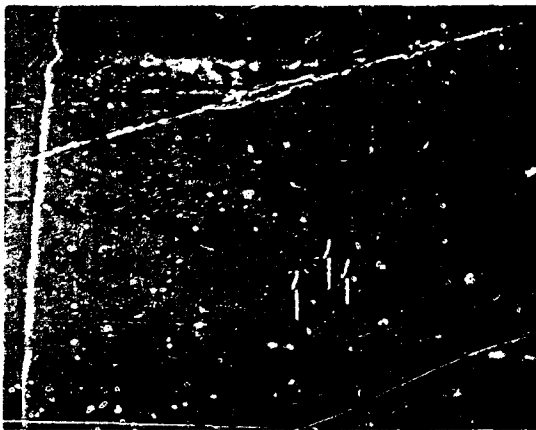
Figure 19. A Sequence of EBIC Displays at the (minus) end of the Conductor Stripe During the Electromigration Test (Taken Off the T.V. Monitor). Void Growth and Void-Particle Interaction are Evident.



(1)



(2)



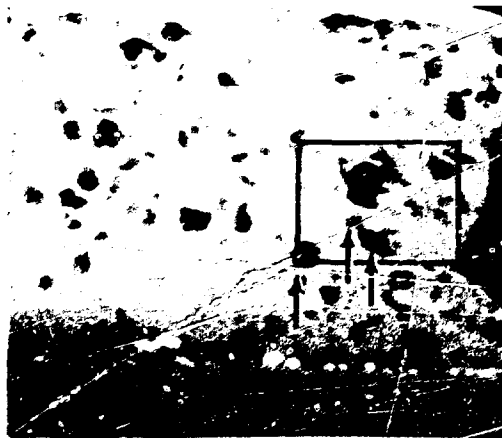
(3)



(4)



(5)



(6)

Figure 20. A sequence of EBIC Displays Taken During the Electromigration Test Showing the Coarsening Process at the (positive) ends

9603-7-1

seem to have the ability to tie vacancies and keep them from coalescing to form large voids. This rate of formation of critical voids is, at present, not included in any of the equations describing electromigration induced failures.

2.8 ELECTROMIGRATION IN TUNGSTEN

Recently ⁽¹⁰⁾ it has been shown that thin films of tungsten can be made with near bulk resistivity ($5.6 \mu\Omega\text{cm}$). Because of its much smaller diffusion coefficient than that of aluminum at semiconductor operating temperatures, tungsten has been predicted to have extremely high resistance to electromigration.

Tungsten, 5500 \AA thick, was vapor deposited onto an oxidized silicon wafer and 1 mil wide by 54 mil long test conductors were patterned. Gold pads were used at each end for the bonding of gold wires. Several runs were made at various temperatures but no evidence of electromigration in tungsten was observed. Failure usually occurred at the gold pads which would thin down and fail. Thus, tungsten is extremely resistant to electromigration.

In all these experiments a fairly large ΔT due to Joule heating was present because of the high resistivity of the test conductors and the high temperature coefficient of resistivity. In order to accelerate the tests, it would be necessary to go to a smaller width test conductor and also improve the bonding pads, (use, for example, platinum). Even then a large ΔT could be present and introduce temperature gradients in the metallization so that extrapolations to normal operating temperatures and current densities could be in error.

(10) Shaw, J. M. and J. A. Amick, "Vapor-Deposited Tungsten as a Metallization and Interconnection Material for Silicon Devices", RCA Review June 1970, pg. 306.

2.9

ELECTROMIGRATION IN GOLD

Gold is another metallization which has better electromigration resistance than aluminum. Although no electromigration experiments using the standard test conductors were performed, tests of the migration resistance of an RF power transistor having gold metallization on PtSi-NiCr-W were made. (ECOM Contract DAAB07-70-C-0172.)

In order to obtain the high current densities, the transistor was forward biased at $I_E = 17.6$ amps and $V_{EB} = 2.4$ volts in an oven set at 195°C . Using this I_E and V_{EB} and a $\theta = 2^\circ\text{C/watt}$, a $\Delta T \simeq 85^\circ$ was calculated giving an operating temperature of 280°C . The unit opened after 50.5 hours of operation. Only slight hillocking was observed and no voids were seen except at the opens. All opens occurred near the emitter bond pads where the current density was 3.8×10^6 amps/cm². This device lasted 90 times longer than that predicted using the best aluminum (large grained-glassed). Tests were attempted on identical devices using normal production aluminum metallization (small grained). It was impossible even to reach the test current and voltage without destroying the device.

2.10

SUMMARY

Electromigration in aluminum and in the aluminum alloys Al-0.75% Mn, Al-0.45% Fe, Al-2% Cu was studied. An engineering curve to predict MTF was obtained for the Al-2% Cu alloy. This alloy has an activation energy of approximately 0.6 eV when $\log \frac{A}{j^2(\text{MTF})}$ is plotted vs $1/T$. The measurements indicate greater

electromigration resistance than "small grained" aluminum at all temperatures, and better electromigration resistance than large grained aluminum above approximately 70° C. Electromigration studies of this alloy were also made in the scanning electron microscope to better understand the mechanisms responsible for the beneficial behavior of Cu additions. It was found that only after a region became depleted in Cu did any voids appear. These voids moved very slowly and were easily tied to θ phase particles.

An RF power transistor having gold metallization on PtSi-NiCr-W was electrically stressed to compare the electromigration resistance of this metallization to that of pure aluminum. The device lasted 90 times longer than that predicted using the best pure aluminum (large grained-glassed).

SECTION III

3.0 SOLID STATE DISSOLUTION OF SILICON INTO ALUMINUM

3.1 INTRODUCTION

Silicon dissolution into the aluminum metallization at contact areas is a potentially very serious failure mechanism. At contact areas a diffusion couple exists. Although aluminum is nearly insoluble in silicon⁽¹¹⁾, silicon has a small solubility in aluminum. Dissolution of silicon into the aluminum metallization occurs during device processing and subsequent high temperature operation. Silicon in the aluminum can affect device performance by creating regions of high resistivity in the metallization. Also, instead of a uniform dissolution, the silicon diffuses into the aluminum from localized areas.⁽⁵⁾ These areas appear as etch pits when the metallization is removed and in certain applications may be deep enough to penetrate an underlying junction in the silicon causing a short circuit.

In the following paragraphs this dissolution process is discussed in greater detail. First, previous work on both the solubility and diffusion of silicon in aluminum is presented. Next, qualitative features of the dissolution process, important to semiconductor devices, are described. Ways to estimate the kinetics of this process at both high temperatures (device processing temperatures) and low temperatures are discussed. Data on the kinetics are also presented using metallographic techniques.

(11) Hansen, M., Constitution of Binary Alloys, 2nd edition, McGraw-Hill, New York 1958.

A coarsening process is described which occurs at the Al-Si interface upon overaging. Some pits in the silicon grow in size while others disappear indicating that aging beyond the time necessary to satisfy solid solubility of silicon in aluminum can be detrimental. All the work presented here was done using aluminum thin films and therefore the results are directly applicable to any semiconductor device with aluminum metallization.

3.1.1 Previous Work

Aluminum and silicon form a simple eutectic system (Figure 21). At the eutectic temperature of 577°C the solubility of silicon in aluminum is 1.59 atomic percent and this solubility drops rapidly with temperature. Figure 22 is a plot of log atomic percent silicon vs $1/T$ of this solvus curve using the data given by Hansen⁽¹¹⁾. The curve is linear from 300°C to just before the eutectic temperature, indicating that aluminum and silicon form a near ideal solution.

The only experimental measurements of the diffusion of silicon in aluminum were made around 1940⁽¹²⁻¹⁴⁾. The diffusivity as determined by Bückle⁽¹²⁾ and by Mehl et al⁽¹³⁾ from 450°C to 577°C is shown in Figure 23. Extrapolation to zero percent solute gives⁽¹⁵⁾

(12) Bückle, H., J. Electrochem 49 (1943) 238.

(13) Mehl, R. F., F. Rhines, K. A. von den Steinen, Metal Alloys 13 (1941) 41.

(14) Beerwald, A., J. Electrochem, 45 (1939) 789.

(15) Smithells, C. J., Metals Reference Book, Vol. II, 4th ed. Plenum Press, New York, p. 662.

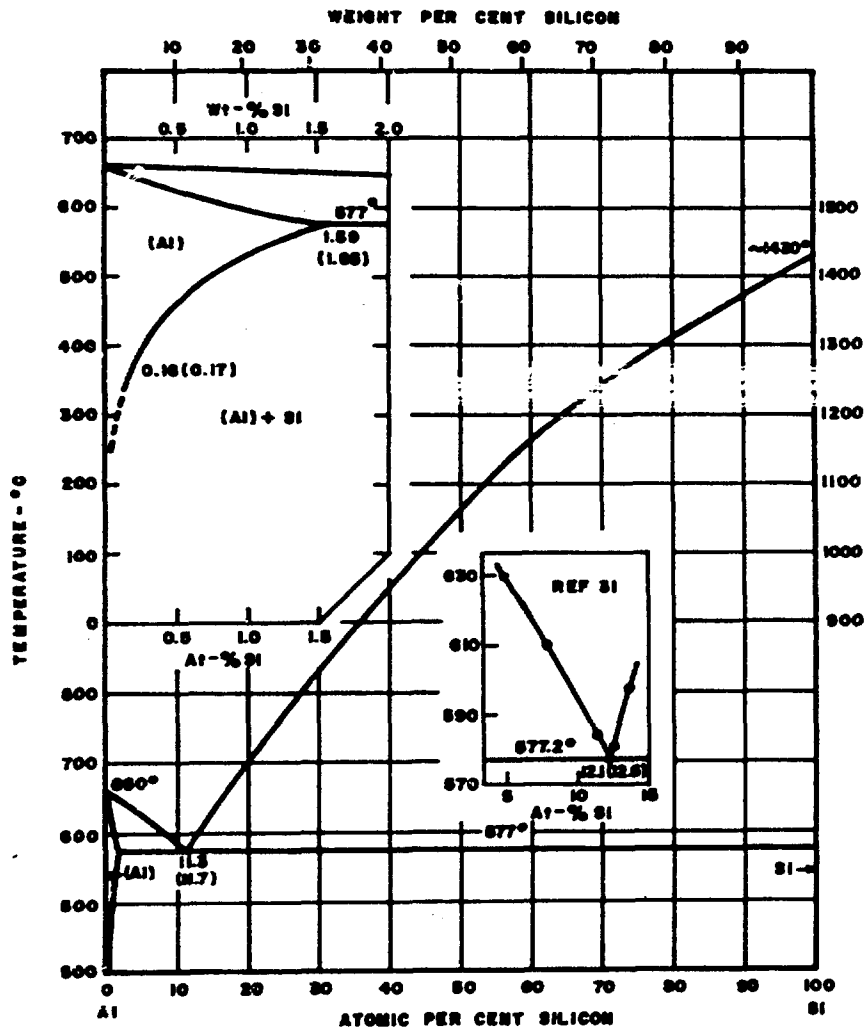


Figure 21. Aluminum-Silicon Phase Diagram
(From Hansen (11))

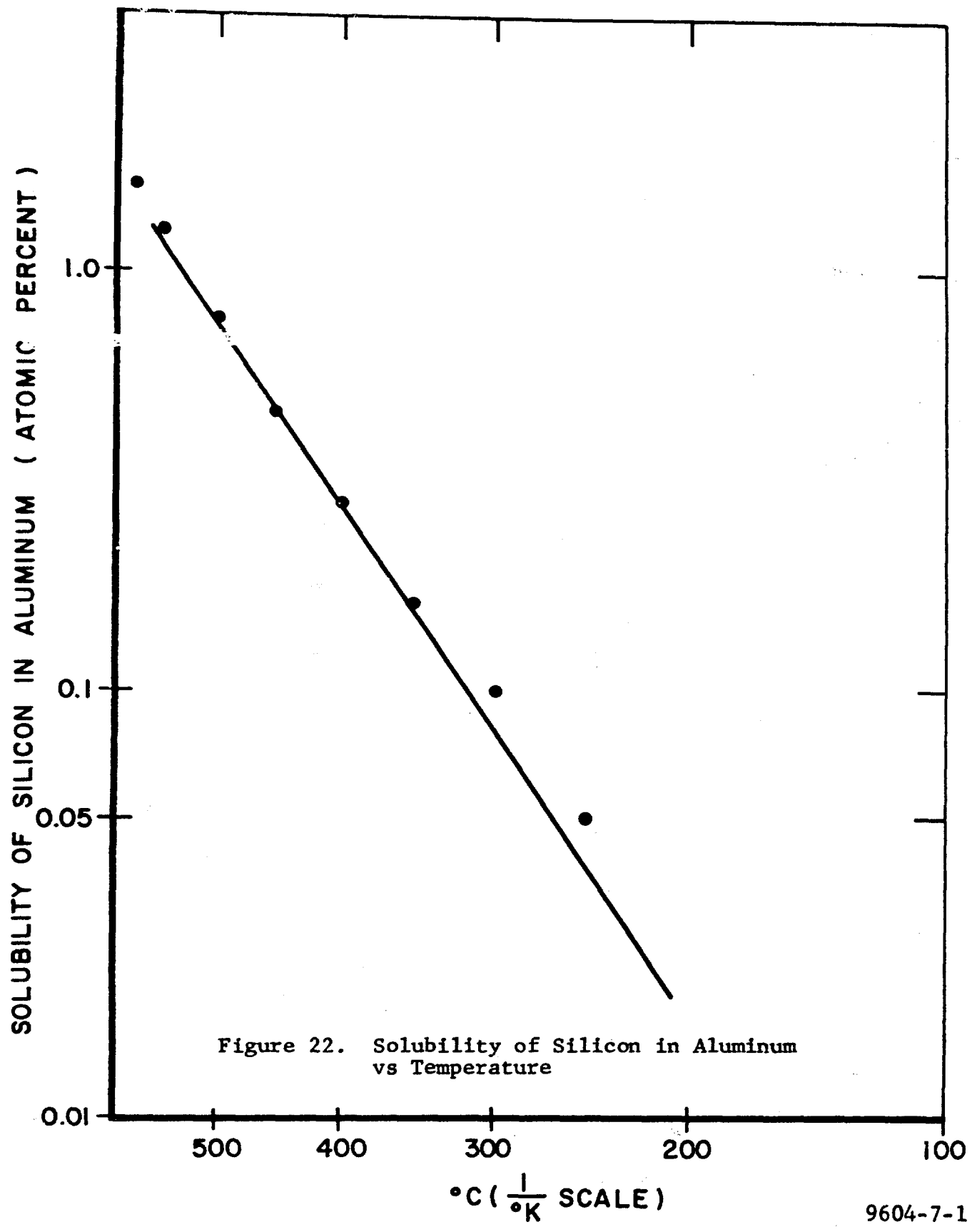


Figure 22. Solubility of Silicon in Aluminum vs Temperature

9604-7-1

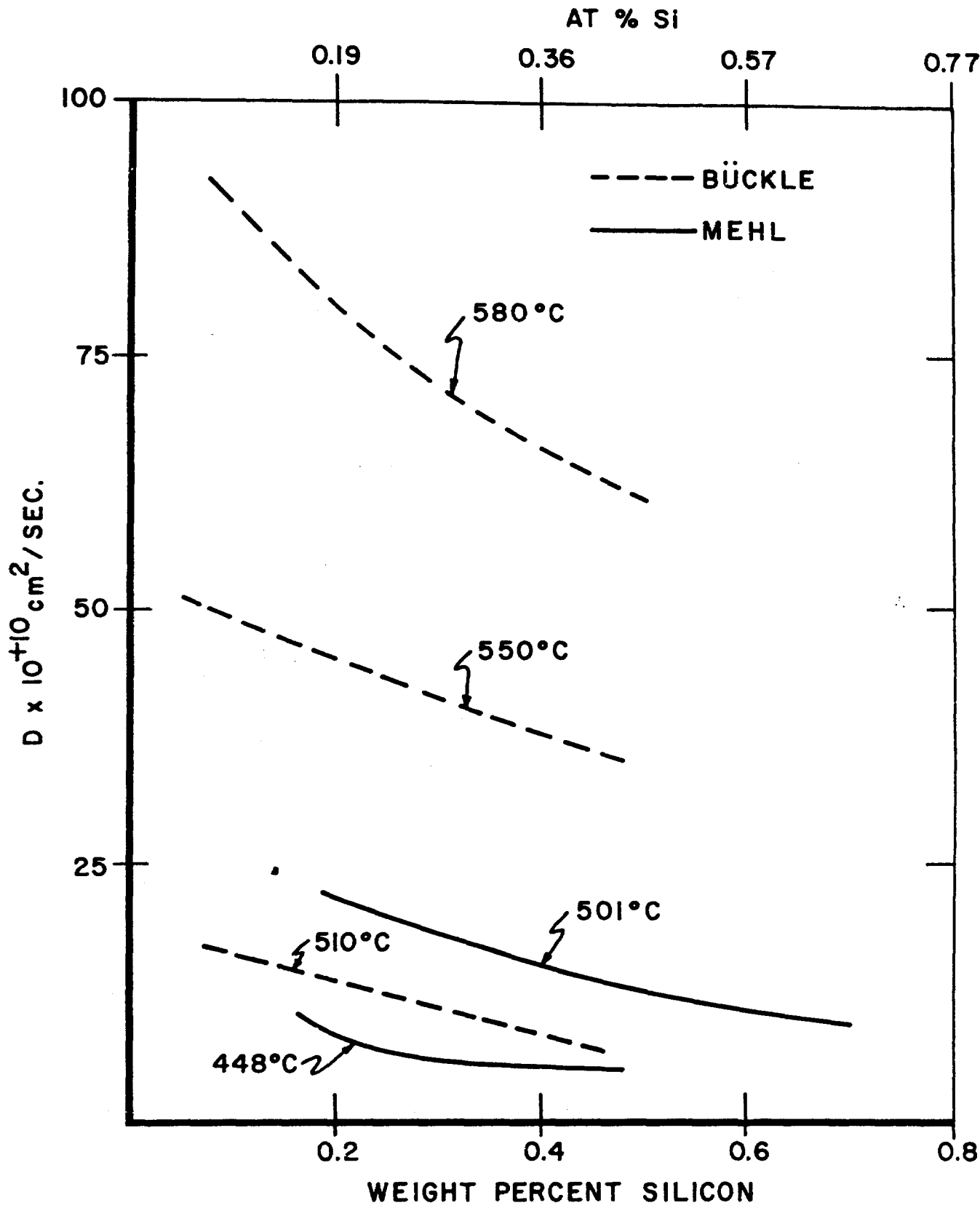


Figure 23. Chemical Diffusion in Al-Si Alloys

$$D \sim 0.9e^{-30500/RT}$$

(16)

However, the extrapolation to lower temperatures may not be accurate, as grain boundary diffusion will become more important. Thus, the only experimental data on diffusion of silicon in aluminum in the temperature range of interest in the semiconductor industry (25-500°C) is at 500°C.

Very little work directly related to semiconductor applications has been reported on the Al-Si system below the eutectic temperature. J. Black⁽⁵⁾ reported the occurrence of etch pits at the Al-Si interface after aging at 500°C. He also showed that electromigration of silicon in the aluminum greatly affected the growth of these pits at elevated temperatures.

J. McCarthy⁽¹⁶⁾ attempted to correlate the nucleation of pits with the emergence of bulk defects. He found no correspondence between the location of Al-Si etch pits and dislocations or stacking faults. He also studied the effect of an oxide film on the Al-Si reaction.

3.2 QUALITATIVE FEATURES OF THE SILICON DISSOLUTION PROCESS

Previous work by J. Black⁽⁵⁾ on the etch pits which form in ohmic contact areas indicated that usually only a few large crystallographically-shaped pits form (instead of many small ones as would be expected if the dissolution process were uniform). The

(16) McCarthy, J., *Microelectron & Reliab.* 9 (1970) 187.

morphology and other aspects of this localized nature of the dissolution process are discussed below.

3.2.1 Morphology of the Etch Pits in <111> and <100> Silicon Substrates

High magnification scanning electron microscope pictures were taken to determine the dimensions of the etch pits. As seen in Figure 24, lateral dimensions are easily determined. However, the pits usually have flat bottoms and measurements of the pit depths, an important parameter in shallow junction devices, requires the measurement of the angle of intersection with the surface and of the length of the side walls of the pits. This could not be done accurately for these shallow pits as at high magnification in the SEM the surface tended to charge, resulting in some blurring. However, by making a replica of the surface and coating it with gold, excellent SEM pictures were obtained. Figure 25 is the SEM picture of a replica made from the pits of Figure 24. The large mesa is the ohmic cut in the oxide while the small triangular pyramids are the etch pits. Their depths can easily be obtained from geometrical relations described below or by tilting the replica approximately 90°. This technique is especially useful when the pits have nondescript shapes, as occurs in highly doped silicon.

This replica technique was used to establish the morphology of pits on <100> and <111> silicon substrates. A replica of a well-shaped etch pit formed by aging <100> silicon (with an aluminum film) for 30 minutes at 500°C is shown in Figure 26. From an x-ray Laue photograph, the orientation of the pit in the silicon substrate was established. By tilting the replica, it was determined that all the side walls made ~55° angles with the surface,

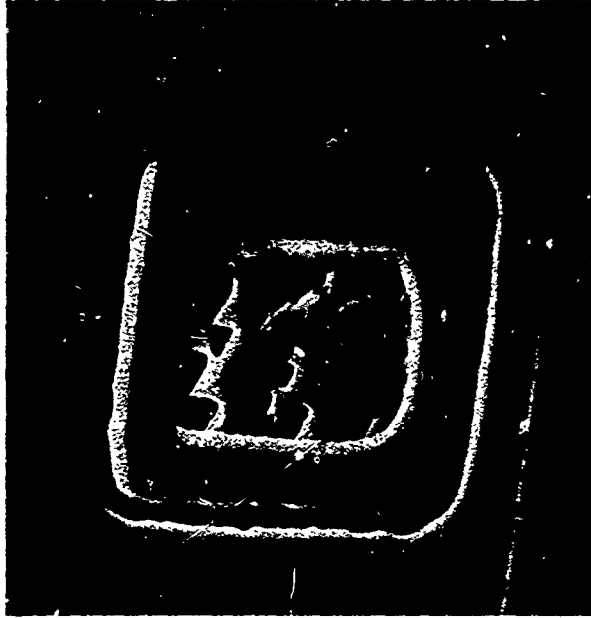
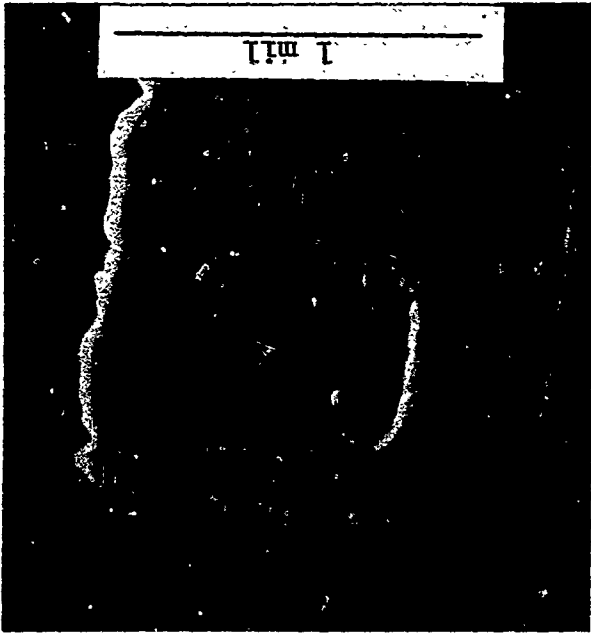


Figure 24. Scanning Electron Microscope Pictures of an Al-Si Ohmic Contact Before and After Removal of the Aluminum Metallization

9606-7-1

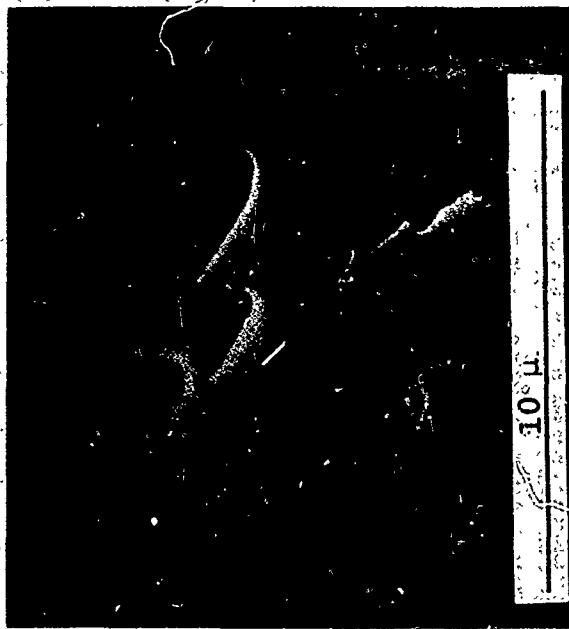


Figure 25. Higher Magnification SEM Picture of Etch Pits in Silicon. SEM Pictures of Replicas, (Two Photos on Right) are of the Same Area as the Regular SEM Picture (Left).

9607-7-1

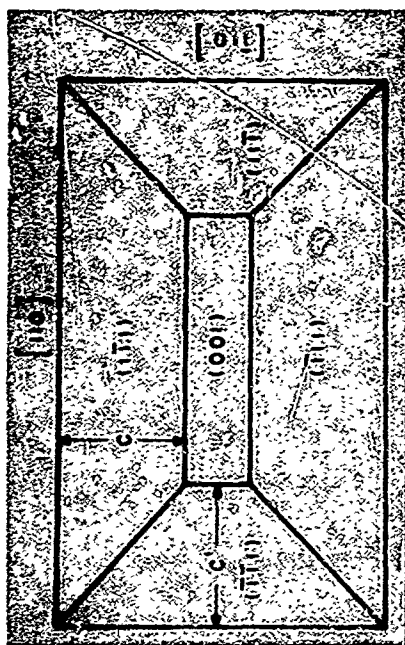
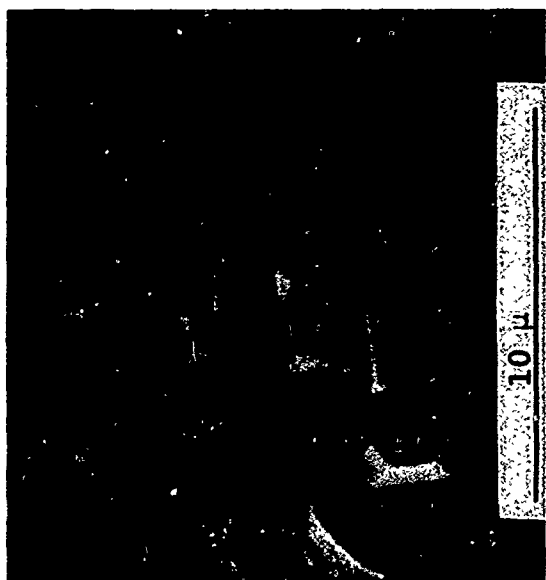


Figure 26. Morphology of an Etch Pit in $\langle 100 \rangle$ Silicon

9608-7-1

indicating they were $\langle 111 \rangle$ planes. A schematic diagram of this pit, indicating its crystallography, is also shown in Figure 26. Since the bottom is usually flat, the depth can be determined by measuring the distance c , giving

$$\text{Depth} = c \tan \alpha' = 1.41 c \quad (17)$$

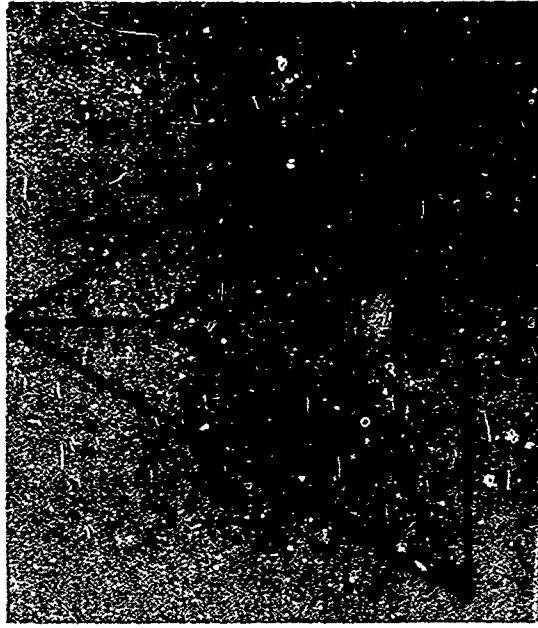
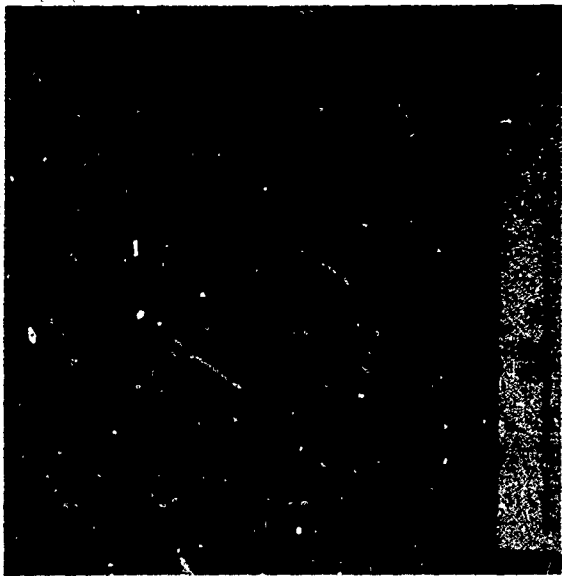
where $\alpha' = 54.74^\circ$ is the angle between $\langle 111 \rangle$ and $\langle 100 \rangle$ planes. The Morphology for pits in $\langle 111 \rangle$ silicon is shown in Figure 27. The pit replica shows the triangular symmetry of these pits. Again, the side walls were $\langle 111 \rangle$ planes but now the flat bottom is also $\langle 111 \rangle$. Here the depth is given by

$$\text{Depth} \simeq c \tan \alpha = 2.82 c \quad (18)$$

where $\alpha = 70.53^\circ$ is the angle between two $\langle 111 \rangle$ planes. For these pits, the bottom was not quite parallel to the surface, since the silicon was off $\langle 111 \rangle$ orientation by approximately 3° .

The above pit shapes are probably the minimum energy configurations since no pits have been found with other crystallographic planes. Experimentally it is also found that pits in $\langle 100 \rangle$ silicon are deeper than pits in a comparable area in $\langle 111 \rangle$ oriented silicon. Pits in $\langle 111 \rangle$ silicon generally have large lateral dimensions and are shallow.

Flat bottomed pits have been seen in other etched materials and have been attributed to small clusters of impurity atoms which have a faster dissolution rate. As soon as the cluster has dissolved away the pit stops growing deeper. This aspect of the morphology has not been studied.



9612-7-1

Figure 27. Morphology of Etch Pits in $\langle 111 \rangle$ Silicon

3.2.2 Location of Etch Pits in Silicon Substrates

The location of etch pits depends on many factors. The most important factor appears to be the general availability of aluminum, as pointed out by Black⁽⁵⁾. Suppose the metallization makes contact with the silicon only along one side of an opening. Silicon on this left side of the contact can enter the aluminum and diffuse down the aluminum stripe, allowing much deeper etch pits to grow. Since the maximum depth (and not the total number of pits) is important in considering shorted junctions in semiconductor devices, these pits near the edge of a contact are then the most critical. At very small Al-Si contacts, one large etch pit, which can extend under the oxide (Figure 28), may form.

Away from the edge other factors may be important in determining pit location. To study the effects of dislocations in the silicon on the location of etch pit formation, x-ray topographs were taken of a 30 Ω -cm p-type <100> oriented wafer before aluminum metallization. One micron of aluminum was deposited and after high temperature aging, the aluminum was removed. The density of etch pits obtained was orders of magnitude greater than the number of observed dislocations which intersected the surface, and thus dislocations are not the determining factor for etch pit location. However, at each dislocation there probably is an etch pit, which would account for approximately one pit out of 400.

A more important influence is shown in Figure 29. The largest etch pits are seen to lie primarily along straight lines which are probably scratch lines made during the final polishing of this wafer (0.1 micron polish). These scratches, which were not observed on the x-ray topographs or in the optical microscope, act as nucleation sites for the pits. When the rate of dissolution

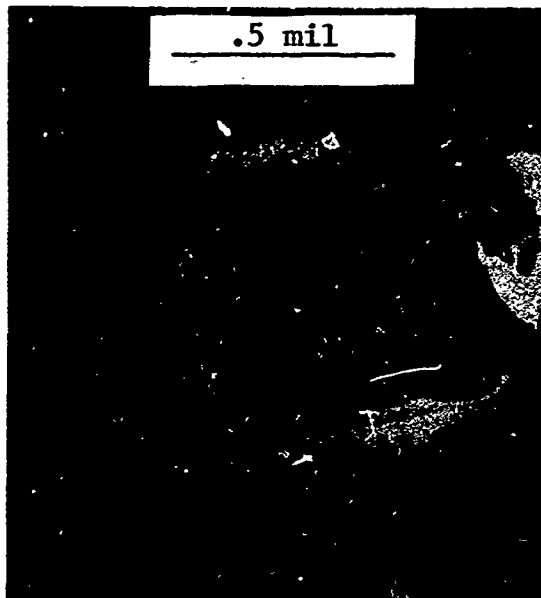


Figure 28. SEM Picture of Pit in Small Ohmic Contact Area Showing Extension Under Oxide

is rapid, it is controlled by the rates of diffusion. However, as the dissolution rate becomes smaller (temperature lower), surface imperfections play a role of increasing importance. Small white clusters of silicon which had diffused into the aluminum are also seen in the SEM photograph in Figure 29.

The location of the aluminum grain boundaries also influences the location of etch pits. This grain boundary effect is most important when the aluminum thin film has large grains. Figure 30(a) shows an SEM picture of the silicon substrate after the aluminum has been removed. The etch pits are fairly shallow and have flat bottoms. The aluminum grain boundaries have been delineated by the precipitated silicon; most pits are near the grain boundaries and triple points, or along the edge of the aluminum film. Also, some pits seem to straddle a grain boundary. Figure 30(b) shows the same effect in another area using the replica technique.

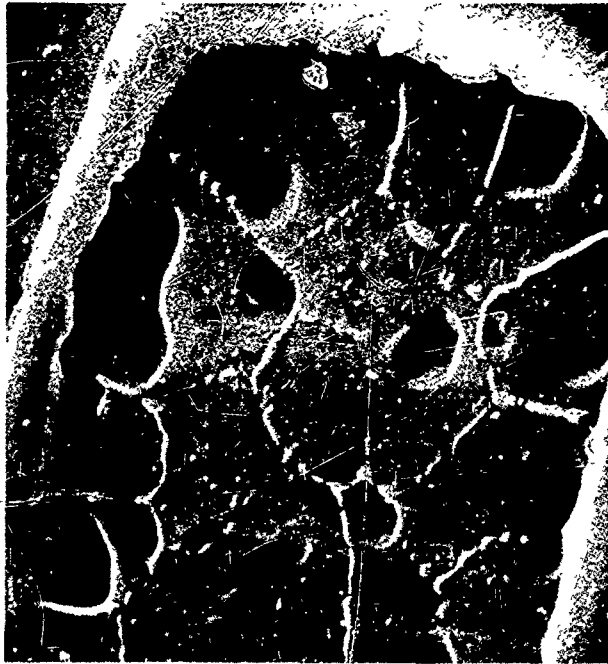
Doping levels in the silicon do not influence the maximum depth of the pits to any great degree. However, pits in highly doped silicon usually are not well shaped (Figure 31).

J. Black⁽¹⁷⁾ showed that electromigration of the silicon in aluminum greatly affected the growth of etch pits at elevated temperatures. The current density introduces an additional driving force for diffusion, causing more silicon dissolution at Al-Si interfaces where the electron flow is into the aluminum and

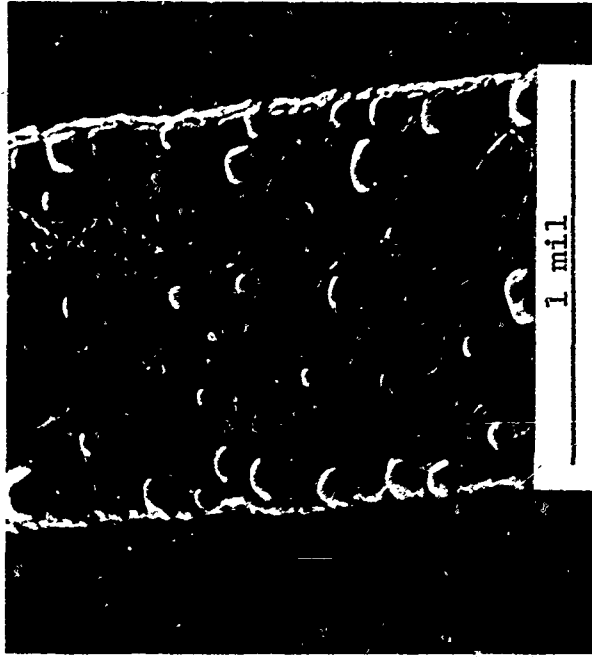
(17) Black, J. R., "Etch Pit Formation in Silicon at Al-Si Contacts due to the Transport of Silicon in Aluminum by Momentum Exchange with Conducting Electrons", Abstract No. 508, Electrochemical Society Meeting, Montreal, August 1968.



Figure 29. Influence of Scratches in the Silicon on Etch Pit Location



(a)



(b)

Figure 30. Influence of Aluminum Grain Boundaries on Etch Pit Location

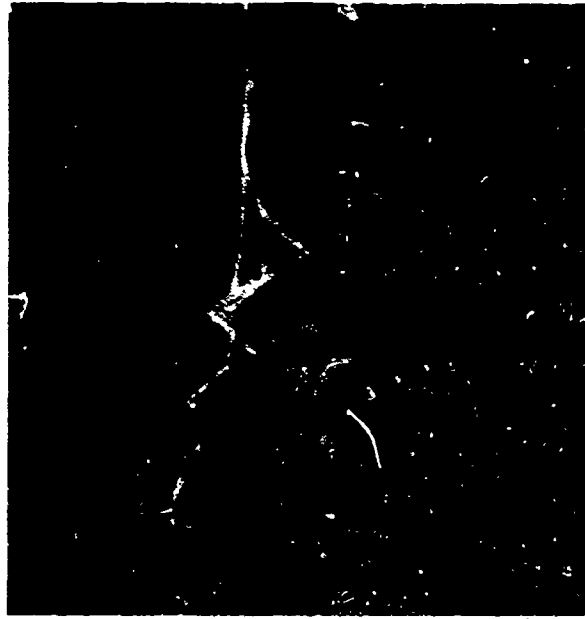
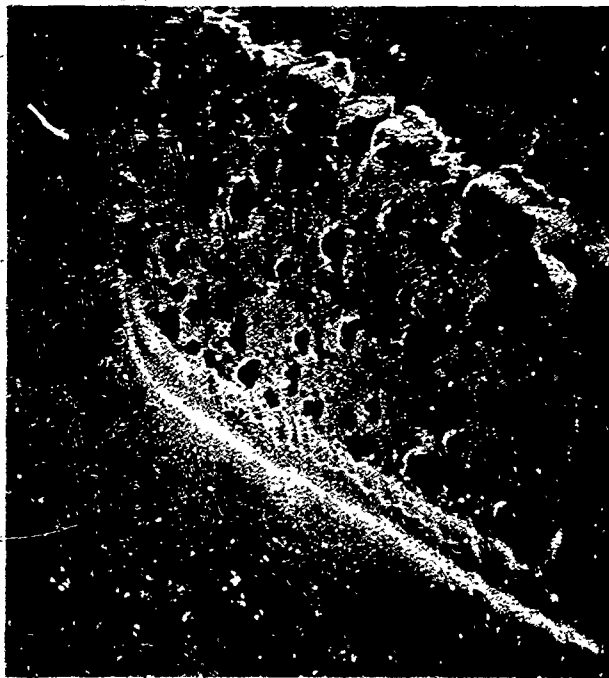


Figure 31. Influence of High Doping on Etch Pit Shape
(Replicas)

9613-7-1

less dissolution when the electron flow is into the silicon (Figure 32). The effect of current crowding at an aluminum-silicon junction can be important during actual operation. A simple electrical analog for the contact area is shown in Figure 33 which demonstrates that the least resistive path is to stay in the aluminum as long as possible. Current densities have been shown to have nearly an exponential behavior with distance from the leading edge of the contact.⁽¹⁸⁾ This current density is an additional driving force for diffusion, and the flux of atoms across the interface will be greatest where this current crowding is the largest.

The location of etch pits may be influenced by several other factors. Stresses between SiO_2 and Si at the edge of an ohmic contact cut may increase the rate of dissolution in this area. Any oxide left at the Al-Si interface will also influence the rate of reaction. This point is discussed in the section on kinetics.

3.3 RESISTIVITY INCREASE OF ALUMINUM WITH ADDITION OF SILICON

The average increase in resistivity of aluminum per wt percent silicon is, from Figure 6,

1.02 micro-ohm-cm in solution

0.088 micro-ohm-cm out of solution

(18) Prokop, G. S., C. Y. Ting, R. R. Joseph, "Current Crowding Effects at Aluminum-Silicon Contacts", 1970 Reliability Physics Symposium, Abstract 4.4, April 8, 1970, Las Vegas

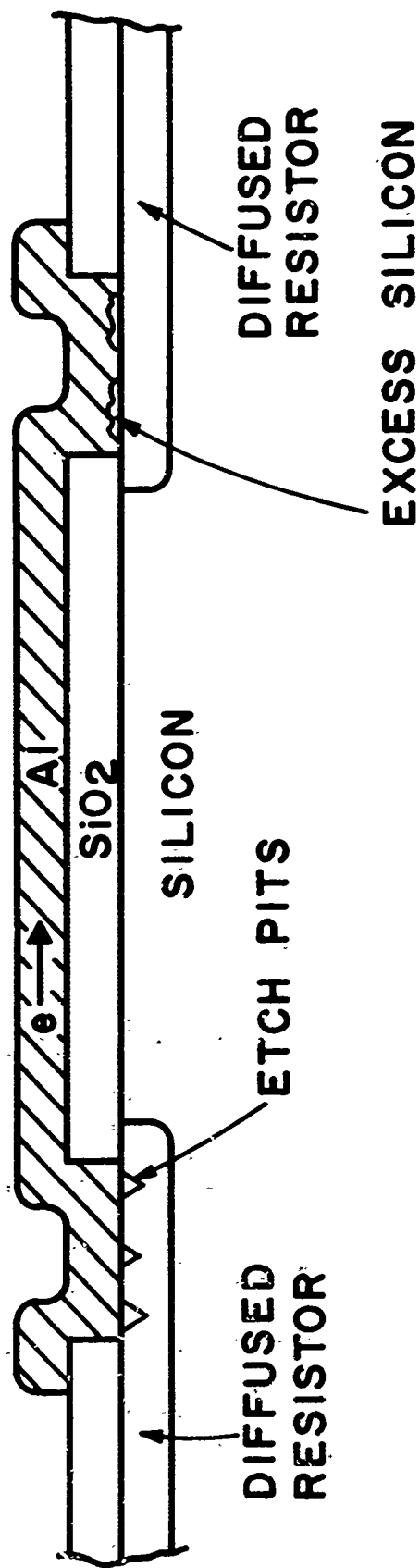


Figure 32. Electromigration Effects on the Silicon Dissolution Process

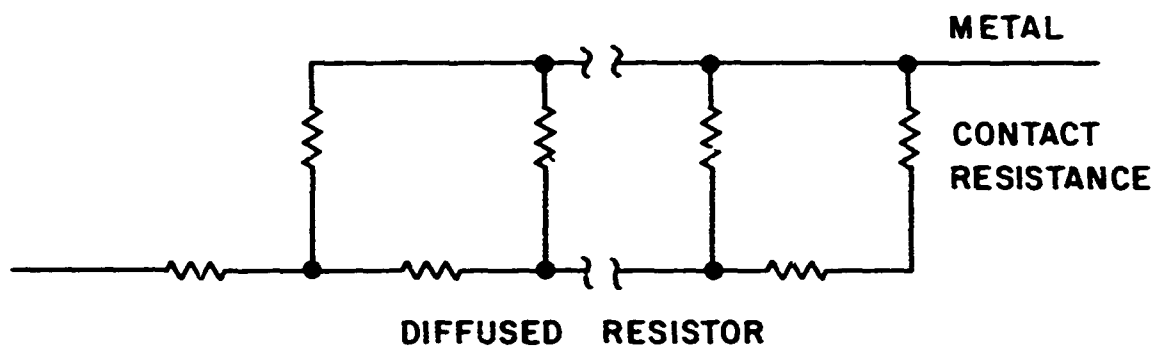


Figure 33. Electrical Analog of Ohmic Contact

Since the solubility of silicon is quite small (Figure 22), the change in resistivity, even when the aluminum has its solubility limit, is usually small. The resistivity change when silicon is out of solution is over a factor of 10 less than when in solution. Thus, if the silicon is distributed randomly, it would be difficult to measure any ΔR . Schnable, et al⁽¹⁹⁾ were unable to detect any ΔR in 2000 Å films of aluminum on silicon even when aged for 500 hours at 350°C.

To account for any change in resistivity in thin aluminum films at temperatures near room temperature, large clusters of precipitated silicon, which extend a significant distance across the stripe, must be present. There must exist external driving forces other than straight diffusion in order to obtain these clusters. Such forces could be thermal cycling and/or electromigration, and may be important after extended periods of time.

3.4 KINETICS OF THE SILICON DISSOLUTION PROCESS

The total amount of silicon dissolution into aluminum as a function of time and temperature depends on the metallization geometry. A good estimate of this amount can be obtained by solving the diffusion equation for an infinitely long stripe of aluminum (actually, only several mils length is required at temperatures below 500°C) coupled to a constant supply of silicon. The amount of silicon which has entered the aluminum in a time t (seconds) per cross sectional area of metallization A is (after a short initial time needed to satisfy solubility directly over the contact area)

(19) Schnable, G. L., R. S. Keen, L. R. Loewenstein, "Study of Contact Failures in Integrated Circuits", Tech. Report No. RADG-TR-67-331, Rome Air Development Center, Air Force Systems Command, Griffiss Air Force Base, New York, Sept. 1967.

$$\frac{N_{\text{Si}}}{A} \simeq \frac{2C}{\sqrt{\pi}} \sqrt{Dt} \quad (19)$$

where N_{Si} is the number of Si atoms, C the solid solubility of silicon in aluminum at temperature T ($^{\circ}\text{K}$) in number/cc, and D the diffusivity at $T^{\circ}\text{K}$. This equation may be rewritten in terms of V_{Si} , the volume of silicon which has entered the aluminum and C_0 , the solubility in atomic fraction as

$$\frac{V_{\text{Si}}}{A} = C_0 \frac{\rho_{\text{Al}}}{\rho_{\text{Si}}} \frac{2}{\sqrt{\pi}} \sqrt{Dt} \quad (20)$$

by using

$$\frac{N_{\text{Si}}}{A} = \frac{V_{\text{Si}}}{A} \rho_{\text{Si}} \quad (21)$$

and

$$C_0 = C/\rho_{\text{Al}} \quad (22)$$

where ρ_{Al} is the number density of aluminum (atoms Al/c.c.Al) and ρ_{Si} is the number density of silicon (atoms Si/c.c.Si). At high temperatures the diffusion coefficient is that of equation 16. However, at lower temperatures grain boundary diffusion, D_{GB} , should become much more important than bulk lattice diffusion. This diffusivity has not been measured. In order to obtain an approximate value for D_{GB} , it can be assumed that

$$Q_{\text{GB}} \simeq Q_{\text{L}}/2 = 15.25 \text{ Kcal/mole} \quad (23)$$

where

Q_{GB} = grain boundary activation energy

Q_L = lattice activation energy

To determine the pre-exponential term of the diffusion coefficient, assume that the lattice diffusion coefficient is equal to the grain boundary diffusion coefficient at about two-thirds the melting temperature of the solvent metal:

$$\begin{aligned} D_{GB} &= D_L \quad \text{at } T = 440^\circ\text{C} \\ D_{GB} e^{-15250/RT} &= 0.9 e^{-30500/RT} \\ D_{GB} &\approx 2 \times 10^{-5} \end{aligned} \quad (24)$$

Thus

$$D_{GB} \sim 2 \times 10^{-5} e^{-15250/RT} \quad (25)$$

At temperatures below 440°C this expression for the diffusivity should be used instead of that given in equation 16 in estimating the amount of silicon dissolution. From equation 20 the amount of silicon dissolution is proportional to the product of the solubility and \sqrt{D} . Both are exponential functions of temperature. By decreasing the highest temperature that the Al-Si couple sees, the overall silicon dissolution can be reduced drastically. The amount of silicon dissolution is also proportional to the cross sectional area of the aluminum metallization (e.g., the total amount of aluminum available).

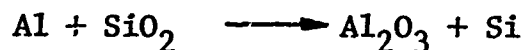
3.5 METALLOGRAPHIC STUDY OF THE SILICON DISSOLUTION PROCESS

In order to study the silicon dissolution process as a function of temperature, a series of aluminum coated silicon chips

was aged for various times at 375°C, 405°C, and 450°C. The wafers were cleaned of oxide by an HF dip prior to evaporation and one micron of aluminum was deposited at a vacuum pressure of 1×10^{-6} torr. After aging, the aluminum was chemically removed to expose the bare silicon surface. This surface was examined with dark field optical microscopy at 800X and micrographs were taken of random areas to study the etch pit formation caused by silicon dissolution. Figure 34 shows three such micrographs taken from chips aged 1210 min., 12900 min, and 22800 min, respectively.

Quantitative metallography techniques were used in conjunction with the micrographs to study the kinetics of the process. The number of pits per unit area, N_A , the areal fraction of pits, A_A , and the diameter of the largest pit, D_L , were determined for each micrograph. Figures 35 through 37 show the results for samples aged at 405°C. It is seen from Figure 35 that the overall dissolution process can be conveniently separated into three stages: (1) an incubation period to penetrate any native oxide which forms, (2) the time required to satisfy solubility of silicon in the aluminum, and (3) a coarsening process whereby the overall silicon solubility remains constant but a few pits grow at the expense of others.

The incubation period before dissolution occurs is brought about by the thin layer of native oxide which forms on the silicon prior to evaporation. The aluminum must first reduce this oxide by the following reaction:



The kinetics of this reaction have been studied as a function of temperature by Black⁽⁵⁾ and are given in Figure 38. It is seen

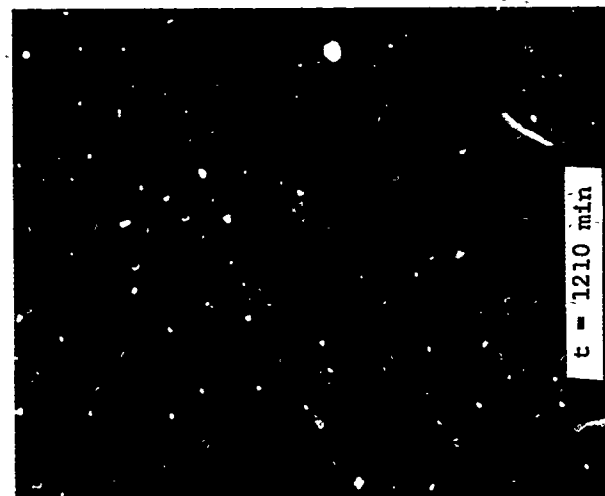
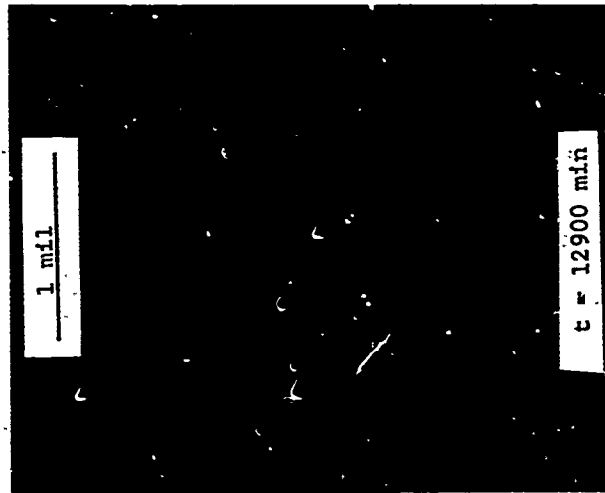
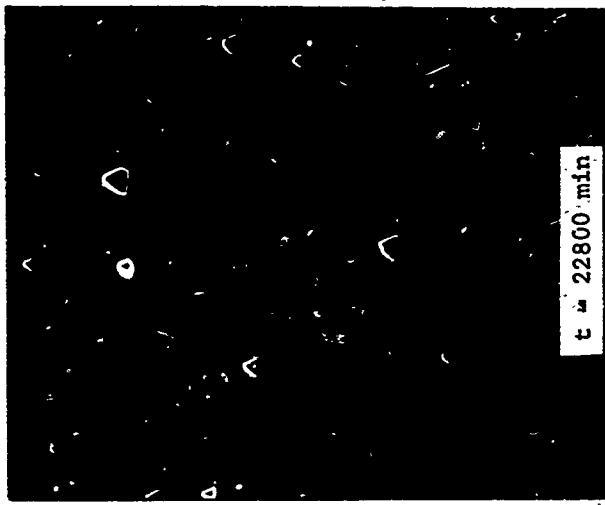


Figure 34. Dark Field Optical Micrographs Showing the Number and Size of Etched Pits in $\langle 111 \rangle$ Silicon After Three Aging Times (405°C). The Aluminum Has Been Removed

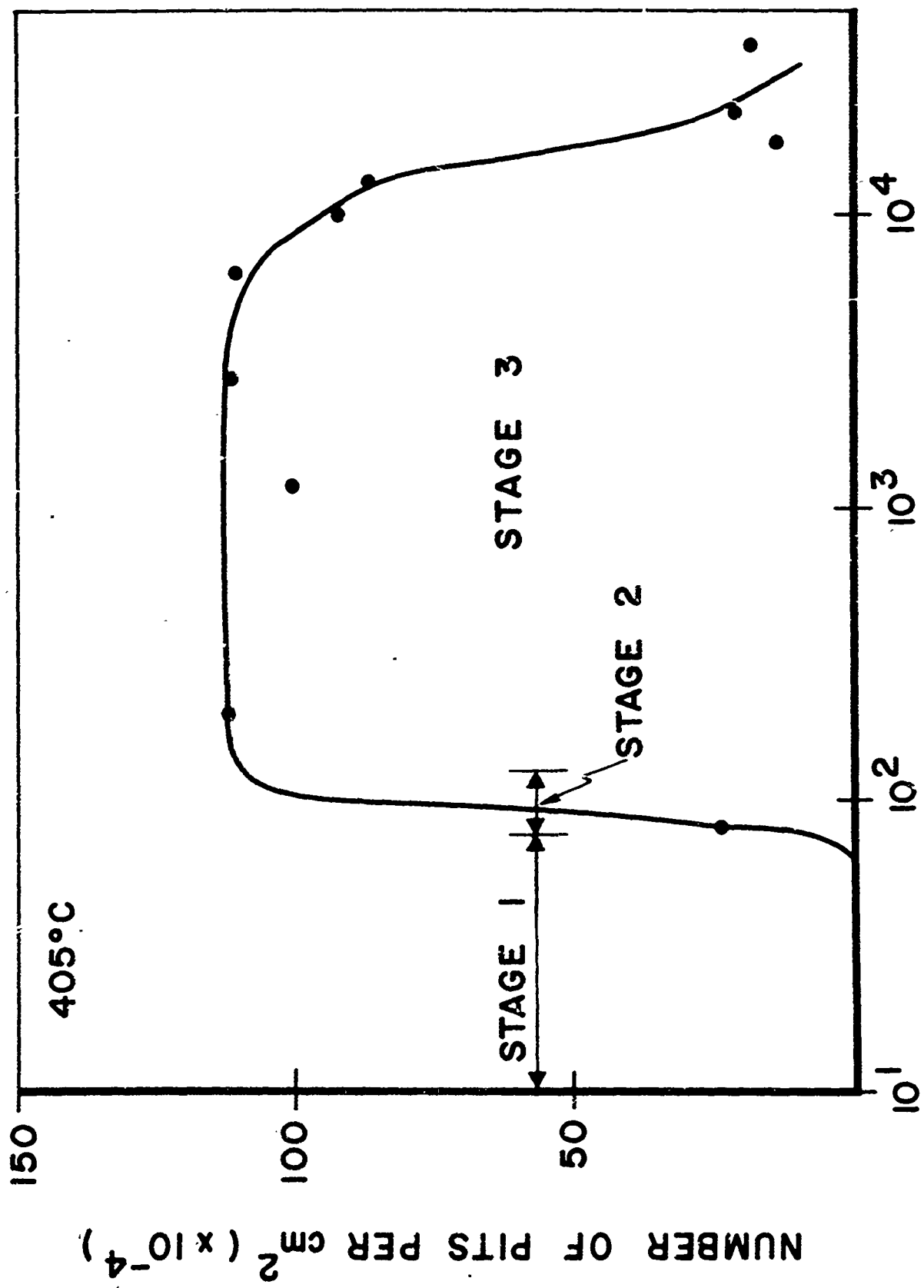


Figure 35. The Number of Pits Per Unit Area vs Time for a Sample Aged at 405°C

9510-5-1

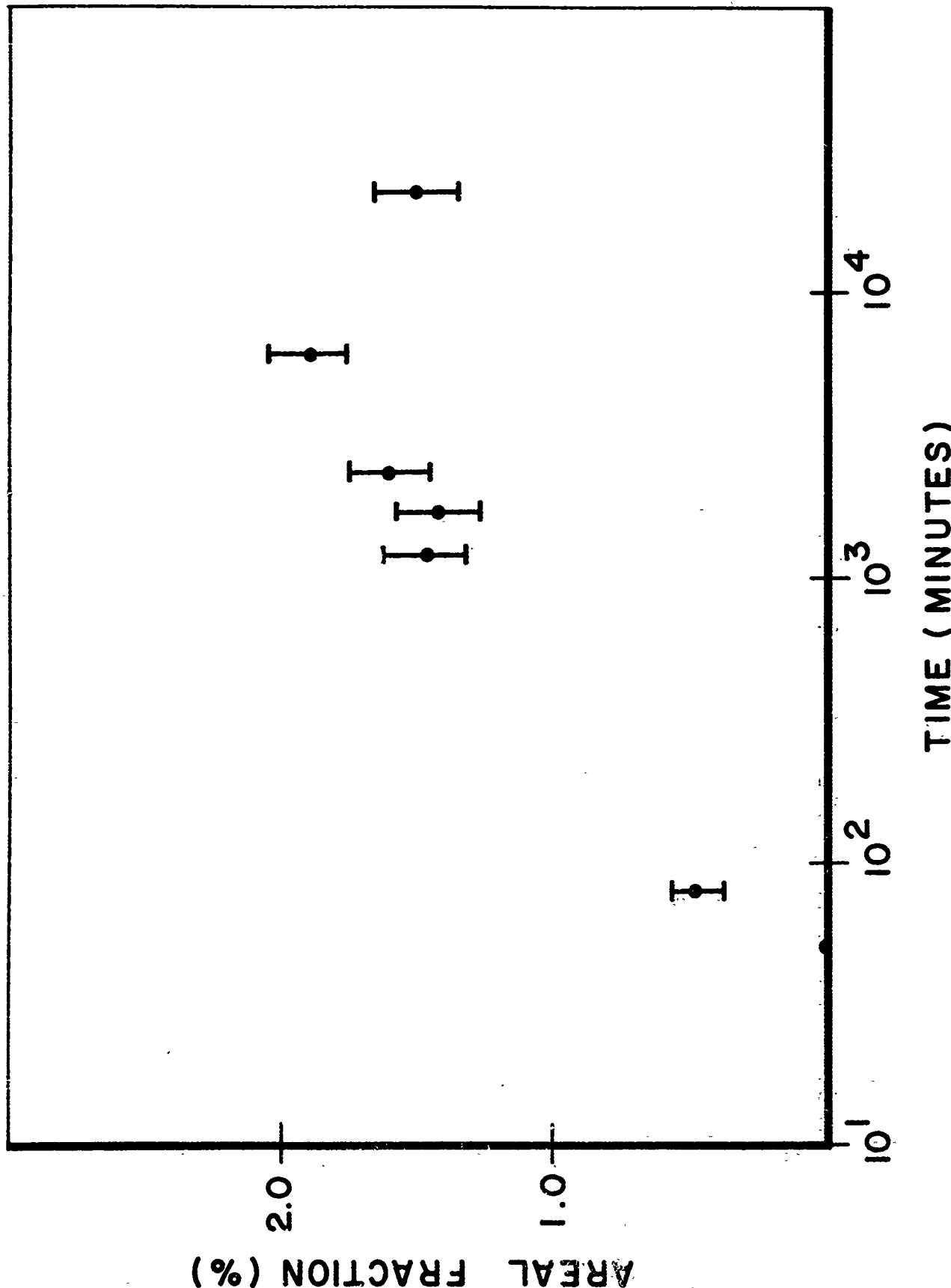


Figure 36. The Areal Fraction vs Time for a Sample Aged at 405°C

9511-5-1

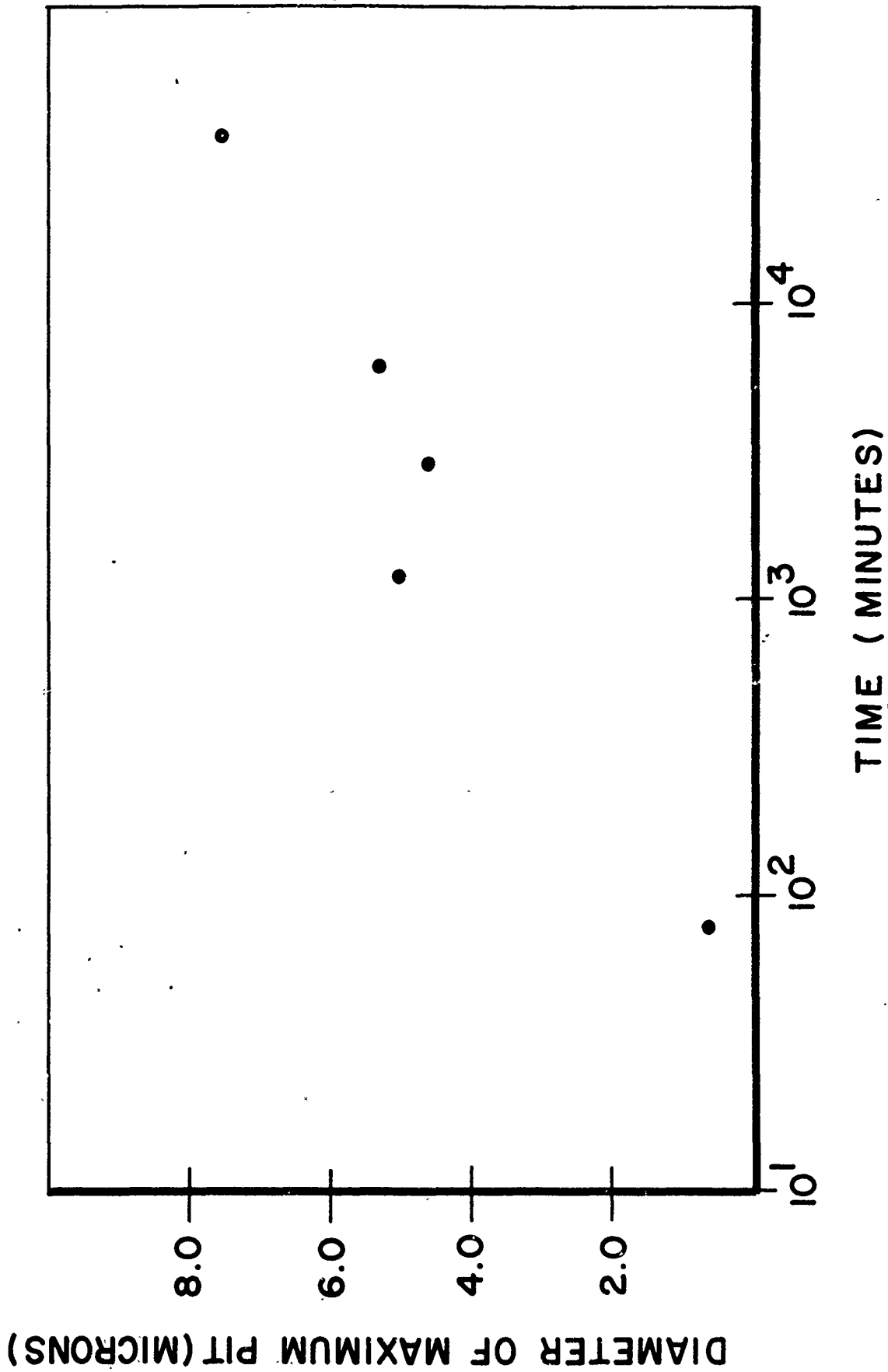
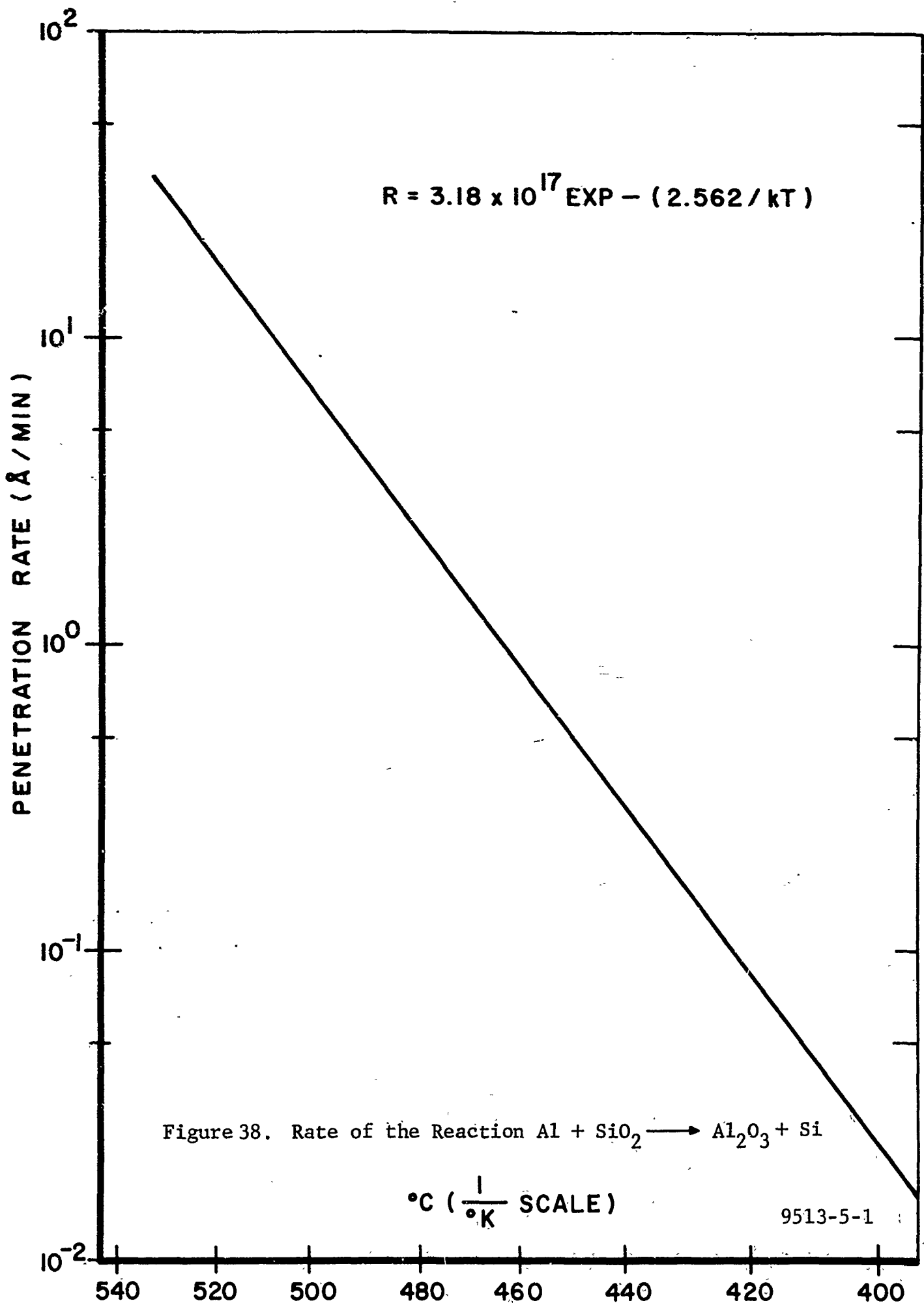


Figure 37. Diameter of the Largest Pit vs Time for a Sample Aged at 405°C

9512-5-1



that above 500°C the kinetics of this reaction are rapid and penetration through the thin oxide skin to allow dissolution can proceed in minutes. However, because of the large activation energy the kinetics slow down perceptibly at lower temperatures. From Figures 35 and 36 it can be seen that it took over an hour to penetrate the native oxide ($\sim 6-10 \text{ \AA}$) which formed on the sample used for the aging studies at 405°C.

The second stage of dissolution involves satisfying the solubility requirement. This can be treated as the diffusion from a semi-infinite piece of silicon into a thin aluminum film of thickness l . The solution to this diffusion equation, which may be given in infinite series form, is shown graphically in Figure 39. The dissolution process is approximately complete when the following equation is satisfied

$$(Dt/l^2) = 1 \quad (26)$$

At 405°C, $D \sim 1.4 \times 10^{-10} \text{ cm}^2/\text{sec}$ from equation 25. Using $l =$ one micron, then $t \simeq 70 \text{ sec}$, which is in agreement with the rapid rise of stage 2 shown in Figure 35. This calculation shows that the time to penetrate any native oxide is the rate limiting step of the silicon dissolution process.

The driving force for the third stage of dissolution -- the coarsening process -- is a reduction of surface free energy per unit volume. In the ideal case minimum surface energy will be achieved by a uniform dissolution. In this case, the maximum pit depth, d , at a given temperature is

$$d = C_{\text{Si}} l \rho_{\text{Si}} / \rho_{\text{Al}} \quad (27)$$

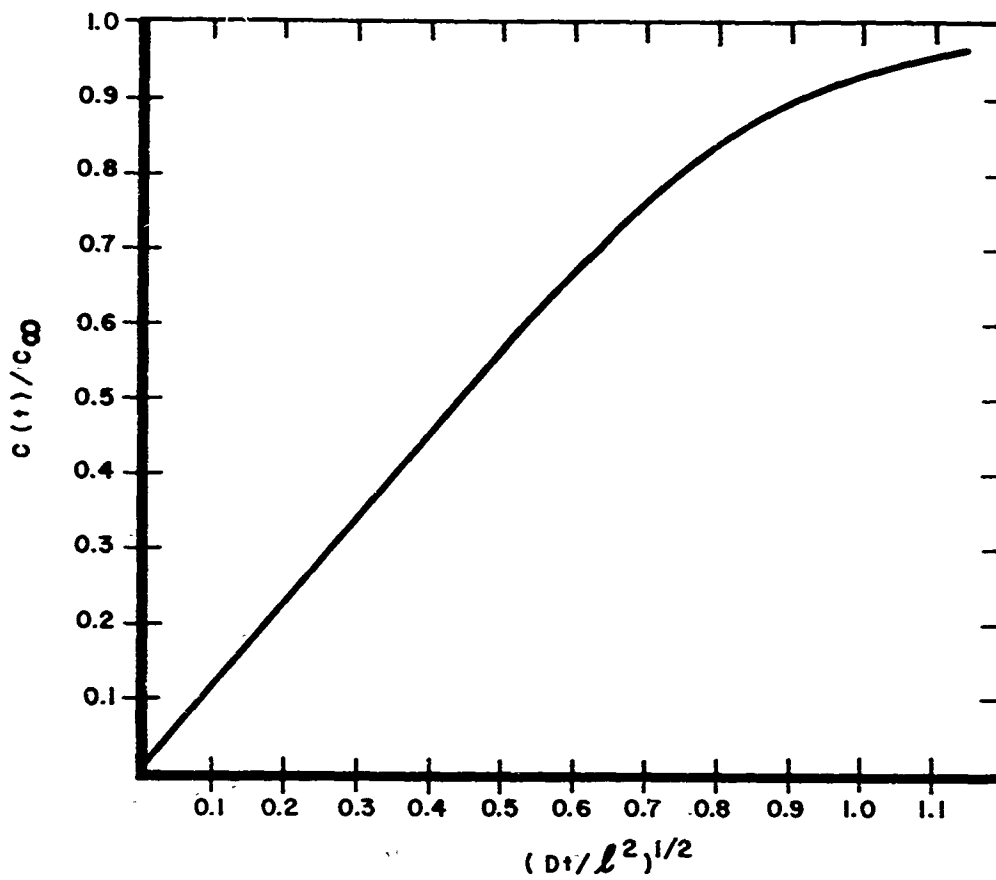


Figure 39. Graphic Solution for Concentration of Silicon in an Aluminum Film of Thickness l , Diffusion Coefficient D and Solid Solubility C_∞ , as a Function of Time t .

where t is the film thickness. In practice, however, as was shown earlier, there is a heterogeneous nucleation of many etch pits instead of the homogeneous interface. In a typical case dissolution may occur only over 1/20 of the total interface area, with the average pit accordingly being 20 times deeper than that predicted by equation 27. Moreover, the surface area/volume is greatly increased in this case of a large number of small pits. The surface area can be reduced if the large pits grow as the neighboring small pits fill in. This coarsening would be analogous to grain growth in materials or precipitate coarsening in two phase materials. Figures 34 and 35 illustrate the coarsening process. It is seen that although the number of etch pits does not change markedly during the early stages of coarsening, the character of the size distribution becomes bimodal. Towards the later stages the number of pits reduces dramatically. The maximum pit diameter increases continuously as shown in Figure 37. Since the pit diameter is proportional to the pit depth, this coarsening reaction can create junction shorting problems and thus the total time at temperature, not just the time required to satisfy solubility, is an important factor.

3.6 SUMMARY

In this work the dissolution of silicon into thin films of aluminum has been investigated. The silicon was shown to dissolve in a non-uniform manner leaving etch pits whose morphology is determined by crystallographic orientation of the silicon. The location of these etch pits was found to be most dependent on the local availability of unsaturated aluminum, with a lesser dependence on damage in the silicon. General equations to estimate the total amount of silicon dissolution into the aluminum metallization

as a function of time and temperature were given. Finally a metallographic study showed that the kinetics of the dissolution process could be conveniently divided into three stages -- (1) an incubation period related to penetration of any native oxide which has formed, (2) the time required to satisfy solubility of silicon in aluminum, and (3) a coarsening process whereby some large etch pits grow at the expense of smaller ones shrinking.

SECTION IV

4.0 SURFACE RECONSTRUCTION OF ALUMINUM METALLIZATION DUE TO THERMAL CYCLING

4.1 INTRODUCTION

Aluminum metallization has been shown to undergo roughening when subjected to thermal cycling. In severe cases, the metal is roughened sufficiently to appear dark under an optical microscope, and its surface contains hillocks similar to those which form during electromigration. Because severe surface reconstruction can result in increasing sheet resistance, can introduce regions of high current density promoting electromigration, and can produce hillocks and whiskers long enough to short to adjacent metallization, the reconstruction can be considered a new type of wear-out failure mode for semiconductor devices.

This section reports on the effects of grain size and alloying elements on thermally-induced surface reconstruction of aluminum films. For reasons which will become apparent subsequently, the reconstruction is classified as occurring in two modes: high temperature-few cycles (device processing) and low temperature-many cycles (device operation). Mechanisms for each of these reconstruction modes are discussed and suggestions for reducing or eliminating this effect are made.

4.1.1 Previous Work

d'Huerle, Berenbaum and Rosenberg⁽²⁰⁾, Paddock and Black⁽²¹⁾, and Santoro⁽²²⁾ have reported surface reconstruction of aluminum films on silicon and SiO₂ after elevated temperature treatments. d'Huerle, et al⁽²⁰⁾ showed that the surface reconstruction took the form of annealing hillocks and whiskers. Paddock and Black⁽²¹⁾ observed that increasing the grain size reduced the number of hillocks that formed. They also noted that the addition of the alloying elements, silicon and silver, increased the number of hillocks but reduced their size, and glassing with SiO₂ over the aluminum totally suppressed surface reconstruction. They attributed surface reconstruction to grain boundary diffusion of aluminum above the recrystallization temperature. Santoro⁽²²⁾ observed that thermal cycling increased the hillock density several times over straight anneals. He reported that the hillocks took three forms: edge hillocks, triple point hillocks, and whole small grain hillocks. He postulated that the formation and growth of hillocks was caused by creep. Sato⁽²³⁾ recently has postulated that the formation of hillocks is controlled by grain boundary diffusion and he showed that small additions of Sn and Mn suppress hillock formation by altering grain size and diffusion rates.

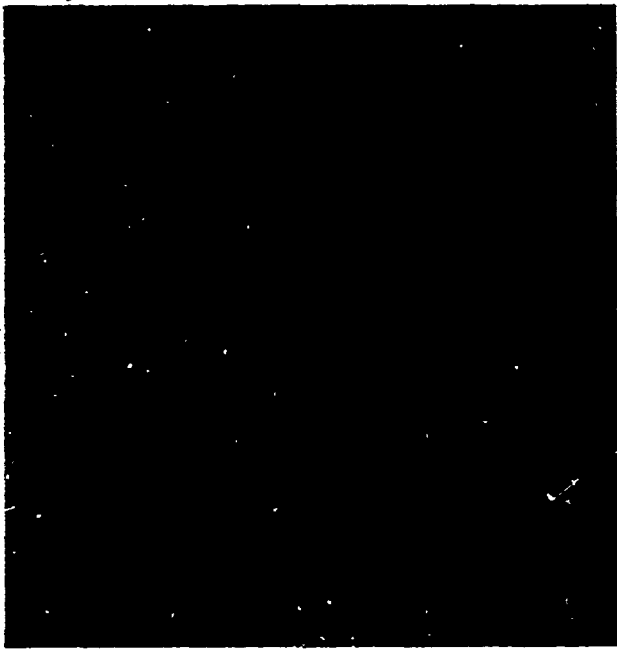
-
- (20) d'Huerle, F., L. Berenbaum, R. Rosenberg, "On the Structure of Aluminum Films", Trans. AIME 242 (1968) 502.
- (21) Paddock, A., J. R. Black, "Hillock Formation on Aluminum Thin Films", presented at the Electrochemical Society Meeting, Boston, May 5-9, 1968.
- (22) Santoro, C. J., "Thermal Cycling and Surface Reconstruction in Aluminum Thin Films", J. Electrochem Soc. 116 (1969) 361.
- (23) Sato, K., T. Oi, H. Matsumaru, T. Okubo, T. Nishimura, "Hillock-Free Aluminum Thin Films for Electronic Devices", Met. Trans. 2 (1971) 691.

4.2 EXPERIMENTAL OBSERVATIONS

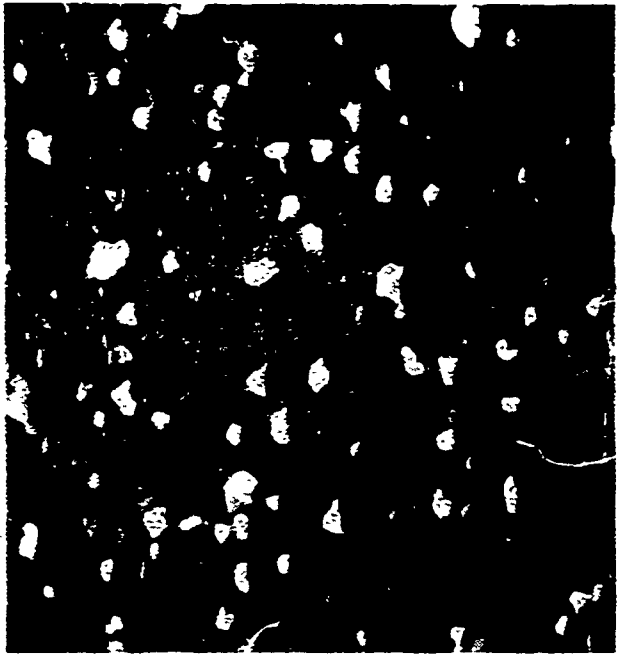
4.2.1 High Temperature-Few Cycles (Device Processing)

A matrix of aluminum thin films 1 μm thick was evaporated on SiO_2 at a vacuum pressure of 10^{-6} Torr in order to learn additional details about the nature of the surface reconstruction of aluminum on silicon and SiO_2 as a function of grain size and alloying elements. The grain size of these films was varied from $<0.5 \mu\text{m}$ to $8 \mu\text{m}$ in diameter by altering the substrate temperatures from 250°C - 400°C and the evaporation rates from $20 \text{ \AA}/\text{sec}$ - $200 \text{ \AA}/\text{sec}$. Also, films containing additions of 2% Cu were prepared, since Cu has been reported to improve electromigration lifetime significantly⁽⁹⁾.

These films were annealed at 250°C and 400°C for $2\frac{1}{2}$ hours to study the effects of long term storage on surface reconstruction at typical device processing temperatures. In order to observe cycling effects (equivalent to a sequence of processes), a fresh set of specimens was cycled ten times for 15 minutes duration/cycle at each of these temperatures. It was noted that the grain size had a great effect on the mode of reconstruction. Fine-grained films ($< 1 \mu\text{m}$) as illustrated by Figure 40 form many large hillocks ($1 \mu\text{m}$ to $5 \mu\text{m}$) covering whole small grains or emanating from triple points. Other grains including many of the larger ones ($> 2 \mu\text{m}$) are observed to be sunken compared to their neighbors. In addition, voids at grain boundaries and along triple points were also seen to form. Both the effect of cycling and of raising the anneal temperature (to 400°C) increased the density of hillocks, voids, and sunken grains by a factor of approximately two relative to a single isochronal anneal at 250°C .



10μ



10μ

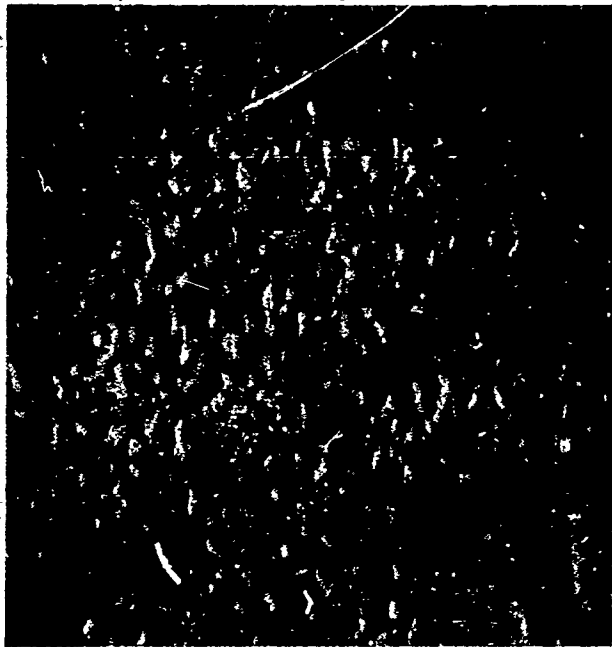
Figure 40. Scanning Electron Microscope Pictures of a Small Grained (<1 micron) Aluminum Thin Film on an Oxidized Silicon Wafer Before and After 10 Cycles for 15 Minutes Duration/Cycle Between 400°C and Room Temperature

As the grain size increases, the number of hillocks and their size decreases as illustrated in Figure 41. They increasingly appeared to emanate from triple points. Voiding disappears and other reconstruction takes the form of wrinkling within certain grains. For the large-grained films (8 μm), as illustrated by Figure 42, only a few very small ($< 1 \mu\text{m}$) hillocks form. The predominant form of surface reconstruction is wrinkling of all grains to varying extents. The pattern appears random with slightly rounded hills and valleys. Temperature affects the magnitude of the wrinkling but cycling appears to have little effect.

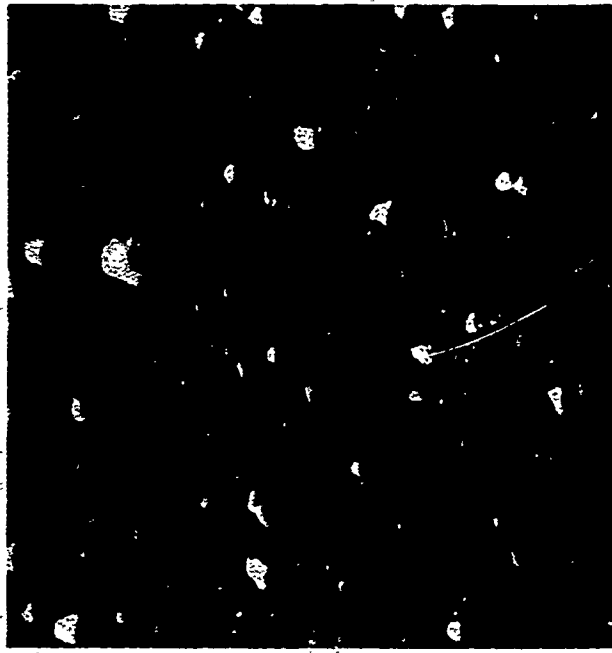
The Al-2% Cu films were found to reconstruct in a different manner from the pure aluminum as illustrated in Figure 43. The films formed many small ($< 0.5 \mu\text{m}$) round hillocks at 400°C, but only very few at 250°C. Electron microprobe analysis presented in Figure 44 showed the mounds to be copper rich indicating these are probably θ phase particles (CuAl_2) which have grown during elevated temperature treatment.

4.2.2 Low Temperature-Many Cycles (Device Operation)

Devices which are required to operate in a pulsed mode with pulse spacing greater than the thermal time constant, or even steady state mode operated devices after many normal on-off operations, have often been observed to have reconstructed surfaces on the aluminum metallization. During these device operations, the metallization will undergo many thousands of temperature cycles, but the absolute junction temperature of the device will never rise above 175°C.

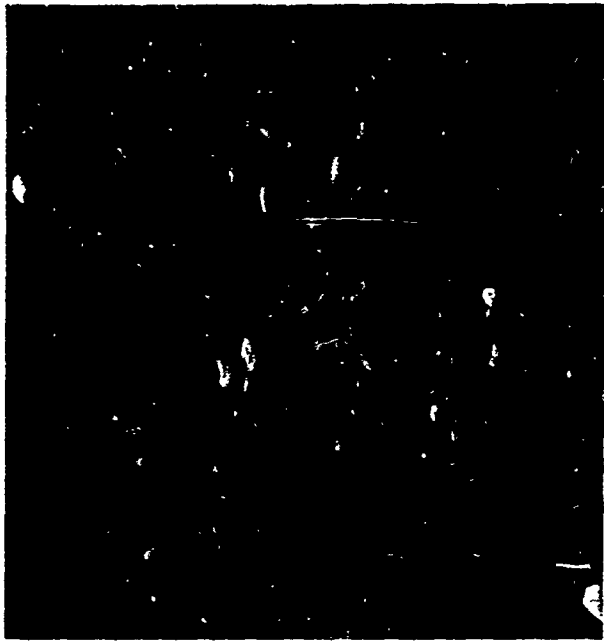


10 μ

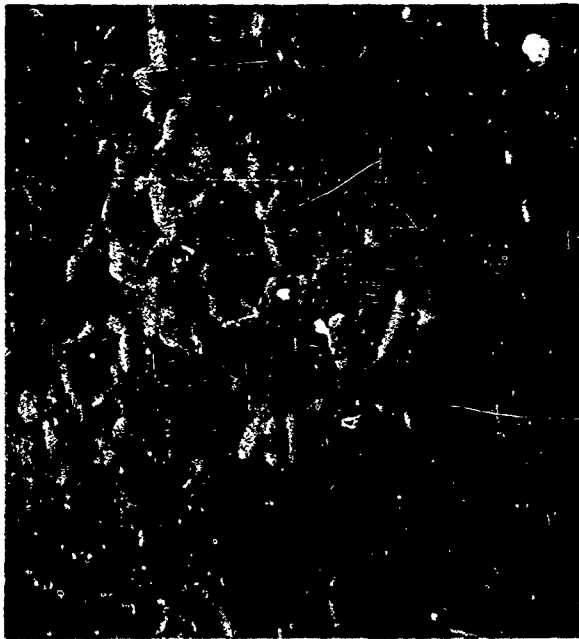


10 μ

Figure 41. Scanning Electron Microscope Pictures of Medium grained (~ 1-2 microns diameter) Aluminum Thin Film on an Oxidized Silicon Wafer Before and After 10 Cycles for 15 Minutes Duration/Cycle Between 400°C and Room Temperature



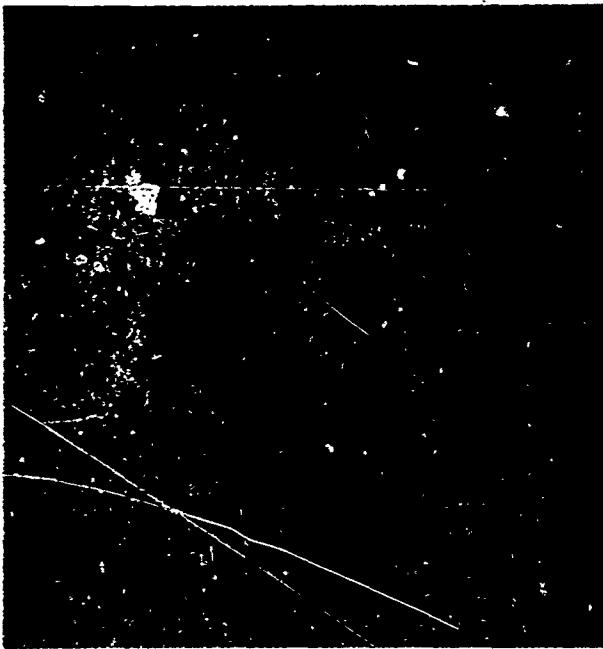
10 μ



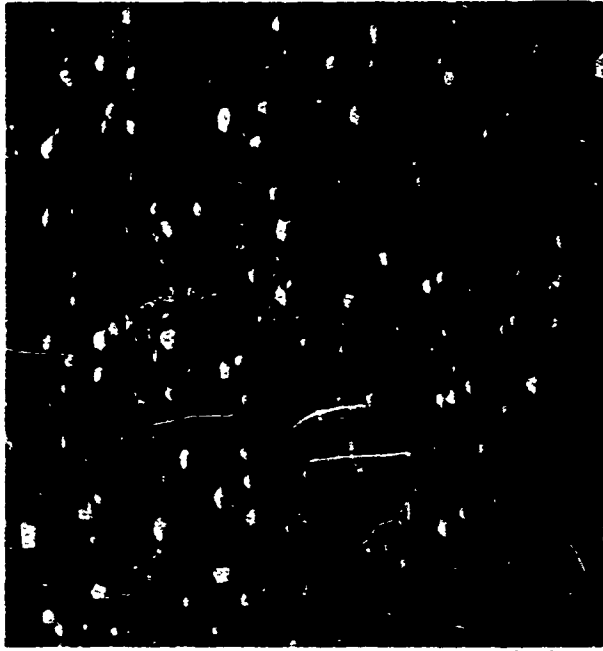
10 μ

Figure 42. SEM Pictures of a Large grained ($\sim 8 \mu\text{m}$) Aluminum Thin Film on an Oxidized Silicon Wafer Before and After 10 Cycles for 15 Minutes Duration/Cycle Between 400°C and Room Temperature

9617-7-1



10 μ



10 μ

Figure 43. SEM Pictures of an Al-2% Cu Thin Film on an Oxidized Silicon Wafer Before and After 10 Cycles For 15 Minutes Duration/Cycle Between 400°C and Room Temperature



Figure 44. Copper X-Ray Images of an Al-2% Cu Thin Film on an Oxidized Silicon Wafer Before and After Aging at 400°C.

In order to study the nature of this low temperature surface reconstruction, one mil wide by one micron thick by 54 mils long aluminum test conductors were prepared on oxidized silicon wafers. These conductors were pulsed electrically with a 10 microsecond square wave pulse and a pulse repetition frequency (PRF) of 10/sec (Figure 45). This rate of pulsing enables the metallization to experience 36000 cycles/hour. During each pulse the temperature of the metallization increased due to Joule heating.

Currents used were between 0.5 to 1.5 amps to obtain Joule heating temperatures between 40°C to 250°C along the stripe. However, the combination of time, temperature and current densities used in these experiments were such that electromigration effects were kept negligible. By using a low duty cycle it was possible to keep the TO-5 header near room temperature throughout the experiment, and the temperature of the test conductor always returned to the header temperature before application of the next pulse. The temperature of the stripe during the pulse was determined using equation 13. The resistance R was obtained by monitoring the voltage across the stripe during the constant current pulse, and the cycle temperature $\Delta T = T - T_0$ was then determined from the maximum $R - R_0$ during the pulse. The major assumption in using this equation to obtain the temperature is that the temperature is uniform along the length of the stripe (i.e., end effects are negligible) during the short pulse. For the long test conductors used in this work, this assumption is believed to be valid.

The effects of grain size on the reconstruction of aluminum films were studied in this manner. Large grained ($\sim 8 \mu$ diameter) aluminum test conductors were observed to wrinkle during testing in specific crystallographic directions in individual grains (Figures 46 through 48). After 36000 cycles at

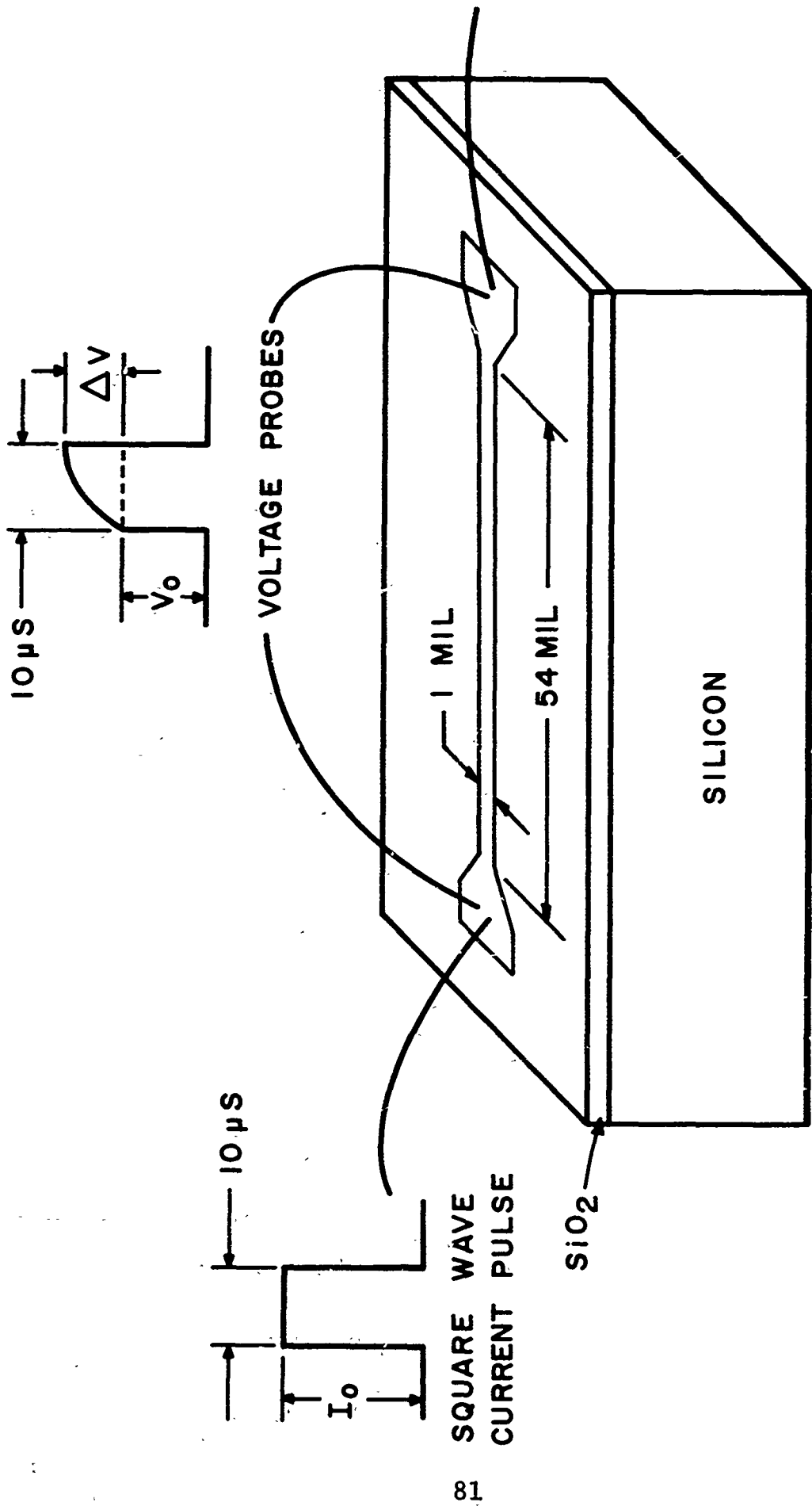


Figure 45. Schematic of Low Temperature-Rapid Cycling Test. The General Pulse Shape is also Shown Indicating The Increase in Voltage Drop as the Stripe Heats Up.



Figure 46. Optical Microscope Photograph of a One Mil Wide Large Grained Aluminum Test Conductor After Low Temperature Thermal Cycling for One Hour. ($\Delta T \approx 70^\circ \text{C}$)

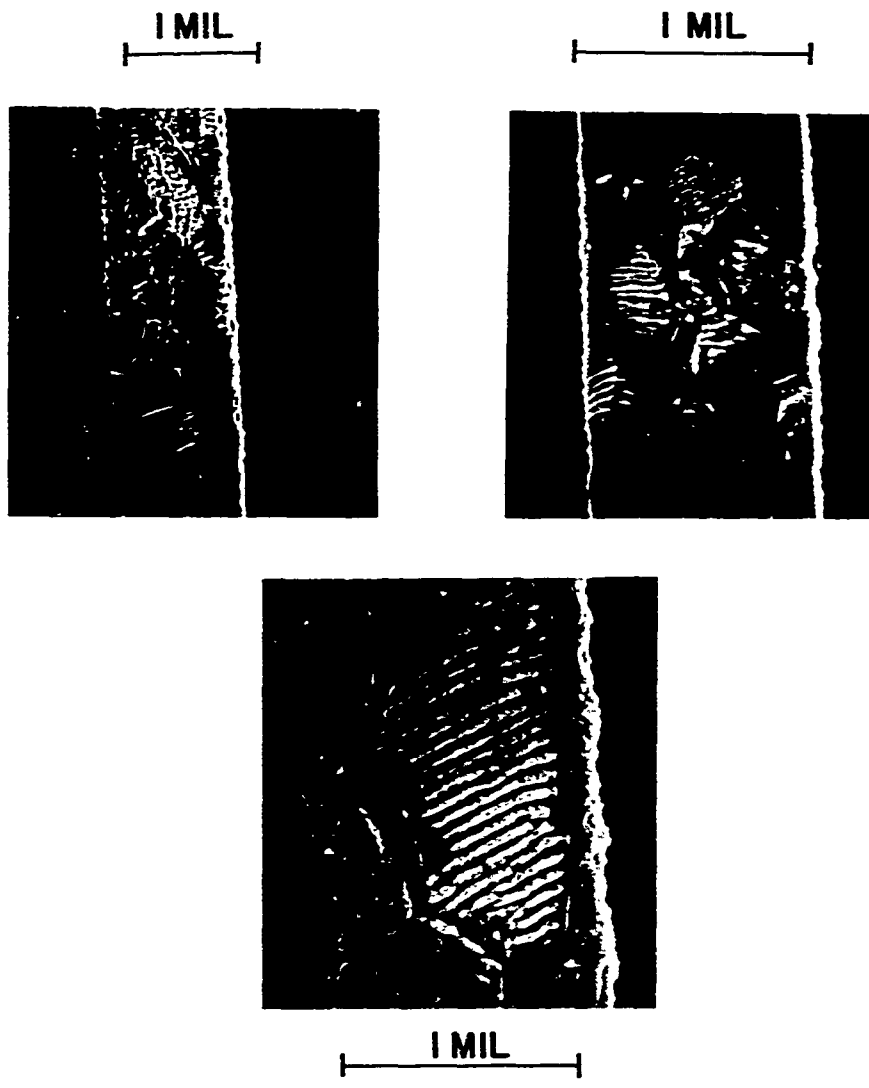


Figure 47. SEM Pictures of Aluminum Test Conductors With Large Grain Size ($\sim 8 \mu\text{m}$) After Low Temperature ($\Delta T \sim 70^\circ\text{C}$) thermal Cycling by Electrically Pulsing



10 μ

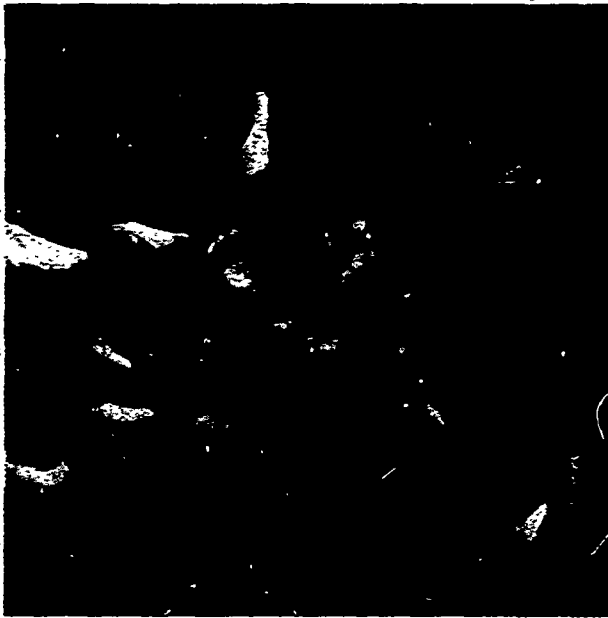
Figure 48. High Magnification SEM Photograph of Thermally Cycled Large Grained Aluminum Showing the Intrusions and Extrusions

9623-7-1

$\Delta T \sim 44^\circ\text{C}$ only certain grains showed this directional wrinkling whereas other grains (presumably at different crystallographic orientations) showed no roughening. The amount of reconstruction is dependent on the number of cycles. After 288,000 cycles at $\Delta T \sim 45^\circ\text{C}$ all grains were wrinkled. There was a fairly rapid increase in the number of wrinkled grains with cycle temperature and for a $\Delta T \sim 78^\circ\text{C}$ the entire aluminum stripe was roughened after 36000 cycles.

Small grained ($< 1 \mu$ diameter) aluminum test conductors were more difficult to roughen by this technique. Below a ΔT of approximately 70°C there was little evidence of metal roughening. At $\Delta T = 100^\circ\text{C}$ most grains showed a slight wrinkling after 36000 cycles and some small hillocks were visible. Figure 49 shows a test device cycled at $\Delta T = 255^\circ\text{C}$ for 36000 cycles by this technique. Severe reconstruction of the aluminum metallization has occurred. This distorted surface appears quite similar to that observed for metallization on a transistor which was temperature cycled by operating the device for 3 minutes on -- 3 minutes off for 20000 cycles at a calculated ΔT of 150°C (Figure 50). This test required over three months compared to the one hour required for 36000 cycles used in the experiments in this study. This illustrates the importance of using ΔT and number of cycles rather than length of service in evaluating the wear-out/potential from surface reconstruction of a device.

Both glassing and alloying were found to retard this low temperature surface reconstruction. A small grained test conductor which has been passivated with 5000 \AA of SiO_2 exhibited no roughening and no glass cracks after 36000 cycles at $\Delta T \sim 135^\circ\text{C}$. Also, an Al-2% Cu alloy film was cycled at $\Delta T \sim 190^\circ\text{C}$ and exhibited no surface roughening.



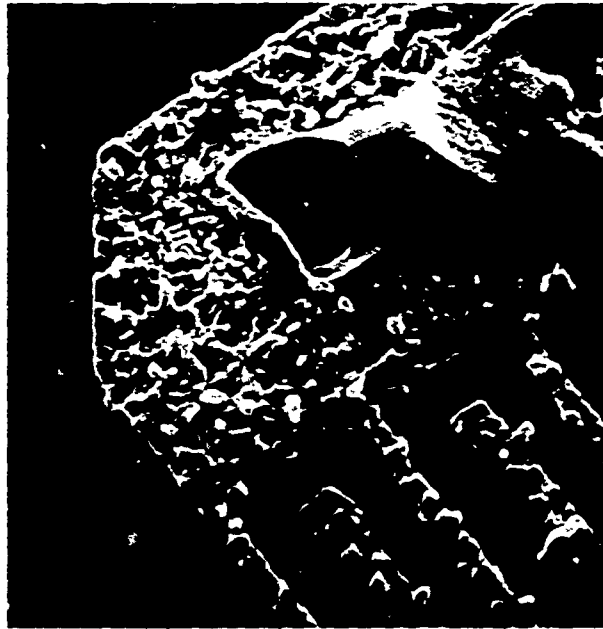
10 μ



1 MIL



Figure 49. Severe Reconstruction Observed in a Small Grained Aluminum Test Conductor After Pulsing 36000 Times With a $\Delta T \sim 255^{\circ}C$



50 μ

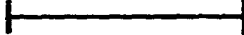
A horizontal scale bar with vertical end caps, indicating a length of 50 micrometers.

Figure 50. Metal Reconstruction Observed on a Transistor After Pulsing the Junction 20000 Times, 3 Minutes on and 3 Minutes Off, at a Calculated Junction Cycle Temperature of $\Delta T \sim 150^{\circ}\text{C}$

4.3

DISCUSSION ON MECHANISMS FOR SURFACE RECONSTRUCTION

Surface reconstruction of thin aluminum films can be seen to occur over a wide range of temperatures when subjected to thermally induced compressive stress cycles. The origin of these stresses has been previously reported (20, 22) to be the thermal expansion coefficient disparity between the silicon or SiO_2 substrate ($\alpha_{\text{Si}} = 3.3 \text{ ppm}/^\circ\text{C}$ or $\alpha_{\text{SiO}_2} = 0.5 \text{ ppm}/^\circ\text{C}$) and the deposited aluminum film ($\alpha_{\text{Al}} = 23.6 \text{ ppm}/^\circ\text{C}$). Moreover, to a first approximation, the magnitude of the stress is proportional to ΔT .

4.3.1 Mechanisms of High Temperature Surface Reconstruction

Previous observers (20, 22) have postulated that diffusional creep is the elevated temperature stress relief mechanism primarily responsible for surface reconstruction. They have given detailed descriptions of how this mechanism could cause hillocks similar to those observed in Figure 40 with grain boundary triple points as preferential nucleation sites. If a certain amount of material is removed from the bulk of the film to the hillock that forms, then the compressive stress is relieved in that local area. As the grain size increases, the density of hillocks decreases further indicating that the grain boundaries are preferential sites for hillock nucleation and growth. However, stress relief still occurs in these larger grains away from triple points but in a more homogeneous manner resulting in gradual wrinkling.

These stress relieved films experience tension upon cooling. Santoro (22) reported the possibility of reordering under tension on cooling leading to grain boundary separation. The

voids observed in Figure 40 at triple points appear to substantiate this postulate. The mechanism would be similar to those which caused the hillock with the stress sign reversed.

The effect of alloy additions to these thin films in general results in a reduction in the degree of surface construction. Alloying will have the dual effect of producing a smaller grain size as well as increasing the yield strength of the film, both of which will retard flow processes. The presence of second phase particles such as Cu or Si in Al will also retard hillock growth since particle growth will also occur during the annealing of the films at high temperatures; the second phase particles can act as effective vacancy sinks and hence retard creep of the parent phase.

4.3.2 Mechanisms of Low Temperature Surface Reconstruction

Diffusional creep cannot account for the observed low temperature reconstruction. Creep is a time dependent phenomenon and the time required for complete stress relief at any specific temperature is given by⁽²⁴⁾

$$t = \frac{\beta (1-\nu)}{KE} \quad (28)$$

where β is a constant ≈ 2.3 , ν is Poisson's ratio, and E is Young's modulus. If volume diffusion rather than grain boundary diffusion predominates K is given by⁽²⁴⁾

(24) Weertman, J., Trans ASM 61 (1968) 681.

$$K \simeq 10 (D/dh) (\Omega/kT) \quad (29)$$

where D is the bulk diffusion coefficient, d is the grain diameter, Ω is the atomic volume, h is the film thickness and k and T have the usual meaning. Taking $d = 8 \times 10^{-4}$ cm for the large grain films, $\Omega = 40 \times 10^{-24}$ cm³, $T = 343^\circ\text{K}$ (70°C), $D = 2.0 \times 10^{-23}$ cm²/sec at 70°C , $\gamma = 0.44$ and $E = 6 \times 10^{11}$ dynes/cm² and $h = 10^{-4}$ cm; the time for complete stress relaxation in the large grained aluminum film at $\Delta T \sim 44^\circ\text{C}$ is $\sim 10^{12}$ seconds. Thus diffusional creep could not have caused the wrinkling since this roughening is observed in a matter of minutes.

Surface reconstruction involves mass transport of metal from one region to another in the film surface. The only possible mechanism of mass transport at these low temperatures is plastic deformation caused by compressional fatigue. Since aluminum does not exhibit a fatigue limit,⁽²⁵⁾ even very small stress levels when applied in a cyclic mode will result in plastic flow and surface reconstruction after a certain number of cycles. The parallel striations observed in the large grained films are probably identical to the characteristic ductile striations observed in the fracture surfaces of fatigued metals⁽²⁶⁾. These striations, called intrusions and extrusions, are a result of the buildup of microscopic slip steps, or slip movements, during fatigue deformation (Figure 51). Each stress or load excursion will produce dislocation motion which will eventually build up into striations of transported metal. Increasing the temperature will assist this fatigue induced plastic flow and the striations will appear at a lower number of cycles.

(25) Dieter, G. E., Jr., Mechanical Metallurgy, McGraw Hill, New York, 1961, pg. 300.

(26) Forsyth, P. J. E., *Acta Met.* 11 (1963) 703.

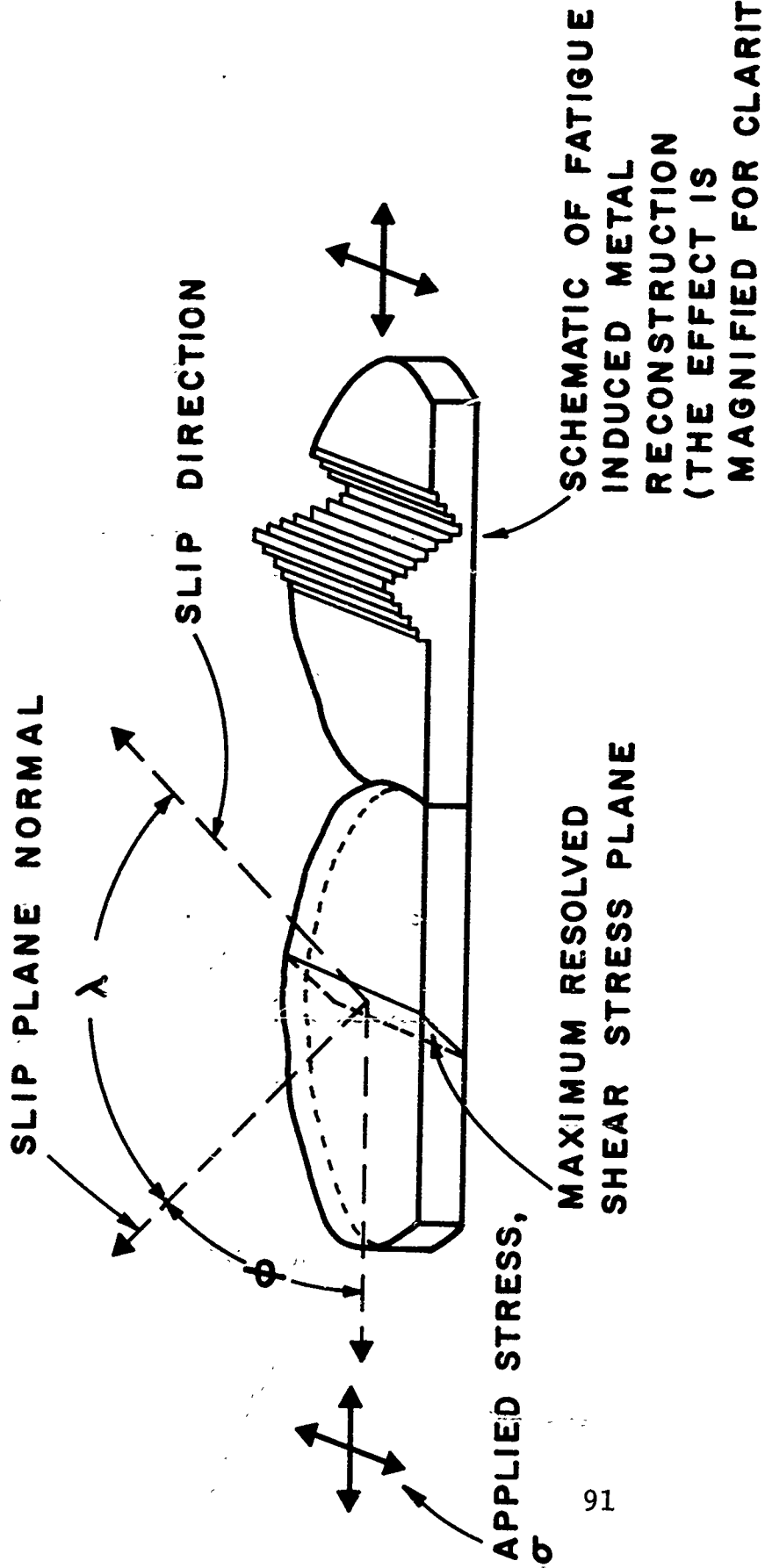


Figure 51. Schematic of Fatigue Induced Metal Reconstruction

The parallel striations shown in Figure 47 result when grains are suitably oriented with respect to the applied stress. Wrinkling will occur in those grains that contain shear planes which experience a maximum resolved shear stress greater than the critical resolved shear stress for plastic flow on that plane. In the event of more than one plane being oriented in such a way as to experience nearly the same resolved shear stress, multiple slip will occur, resulting in the cross hatched pattern seen in some grains in Figure 47.

At high temperatures where diffusion rates are sufficiently high, diffusional creep can be a contributing flow mechanism although high temperature plastic deformation involving conservative motion of dislocations (as opposed to non-conservative dislocation motion during creep) is a possible deformation mode. With increasing ΔT the stress level on the film increases while the yield stress decreases with the result that plastic flow becomes easier.

4.4 SUMMARY

Surface reconstruction of aluminum metallization -- a new potential wearout mechanism -- has been observed to occur under a wide range of conditions. At high-temperature-few-cycles such as might occur during device processing the mechanism for reconstruction is probably diffusional creep. In small grained films the reconstruction is manifested in the form of many large hillocks and whiskers emanating from triple points and whole small grains. As the grain size increases, the number of hillocks and their size decreases and the manner of reconstruction shifts to wrinkling within individual grains. The effect of adding

alloying elements such as silicon, copper and Ag to the aluminum also reduces the hillock size. In the case of copper, the small round hillocks were found to be copper rich, indicating that the particles growing from the surface were probably θ phase (CuAl_2).

Surface reconstruction can also occur at low temperatures after many cycles, such as might occur under certain types of device operation. The mechanism in this case is believed to be compressional fatigue. Large grained films were most susceptible to this wearout mode. They reordered at temperatures as low as $\Delta T = 44^\circ\text{C}$ by forming parallel striations within individual grains. Small grained films had a higher resistance to this type of cycling with evidence of reordering only above $\Delta T = 70^\circ\text{C}$. The reordering in small grains took the form of hillocks and whiskers. For both large and small grained films as the temperature difference and/or the number of cycles increased, the extent and severity of the reconstruction increased. Since severe reconstruction can cause resistance changes, can introduce regions of high current density promoting electromigration, or can cause short circuits between adjacent metallization stripes, it can be considered as a new wearout mechanism. This reconstruction can be reduced or eliminated, however, by glassing over the stripes or by the addition of alloying the elements such as copper which increase the fatigue resistance.

SECTION V

5.0 CONCLUSIONS AND RECOMMENDATIONS

The objectives of this research were to study the effects of high temperature and high current density on the physical properties of aluminum metallization. This work was concerned with three possible failure modes of the metallization; electromigration, interdiffusion of silicon and aluminum, and metallization reconstruction due to thermal cycling.

5.1 ELECTROMIGRATION

Electromigration was studied in aluminum and in the aluminum alloys Al-0.75% Mn, Al-0.45% Fe, and Al-2% Cu. The Al-2% Cu alloy was found to have the best median time to failure (MTF) of the aluminum alloys studied. MTF as a function of current density, temperature, and cross-sectional area was obtained for this alloy. The data indicate this metallization would offer substantial improvement over pure aluminum with respect to electromigration on RF power transistors. This alloy was also studied extensively using the scanning electron microscope. A possible mechanism for the beneficial behavior of copper was obtained.

Although much work has been done to obtain MTF curves for a particular metallization, many of the basic mechanisms which

ultimately cause a metal conductor to open are not fully understood, and should be studied more. Why do voids coalesce at a particular location in the metallization? Can the effect of alloying additions on MTF be predicted from theory? How important are temperature gradients in the metallization?

5.2 SILICON DISSOLUTION

Silicon dissolves into aluminum metallization in a non-uniform manner leaving etch pits whose morphology is determined by crystallographic orientation of the silicon. The location of these etch pits was found to be most dependent on the local availability of unsaturated aluminum. Other factors such as damage in the silicon, aluminum grain boundaries, and doping levels of the silicon are also discussed. General equations to estimate the total amount of silicon dissolution into the aluminum metallization as a function of time and temperature are given. A metallographic study showed that the kinetics of the dissolution process could be conveniently divided into three stages:

- (1) An incubation period related to penetration of any native oxide which has formed.
- (2) The time required to satisfy solubility of silicon in aluminum.
- (3) A coarsening process whereby some large etch pits grow at the expense of smaller ones shrinking.

Silicon dissolution and etch pit formation become a more important reliability problem as geometries get progressively

smaller. Ways of making the dissolution process more uniform and thus decreasing the depth and lateral penetration of the etch pits should be pursued.

5.3 SURFACE RECONSTRUCTION DUE TO THERMAL CYCLING

Surface reconstruction of aluminum metallization was observed to occur under a wide range of conditions. The reconstruction was divided into two parts: high temperature-few cycles (device processing) and low temperature-many cycles (device operation). The effect of aluminum grain size on surface roughening was discussed. The Al-2% Cu alloy was also studied in conjunction with pure aluminum and found to reconstruct less than pure small-grained aluminum in all cases. The possibility of surface reconstruction of aluminum metallization at low cycle temperatures had not been previously recognized. This form of surface roughening becomes more important as devices are operated and cycled at high temperatures. The mechanism for this low temperature reconstruction is believed to be compressional fatigue. More work should be done to gain a greater understanding of this mechanism. Reliability problems related to operating devices at high current densities and, at the same time, subjecting the metallization to thermal cycling should also be studied. The roughened metal surface introduces regions where the current density is even greater than normal, accelerating any electromigration effects.

5.4 TUNGSTEN METALLIZATION

A few electromigration experiments were performed using tungsten metallization on SiO_2 . It was not possible to cause the metallization itself to fail. Failure usually occurred at the gold pads which were necessary for bonding. Studies using tungsten

should be continued as it has many other advantages over aluminum as a metallization for RF power devices. Silicon dissolution into tungsten is negligible. Tungsten is extremely hard, thus greatly reducing any possibility of mechanical damage. Also its thermal expansion coefficient almost matches that of silicon and SiO_2 , greatly reducing stresses which cause surface reconstruction. Tungsten, however, has some disadvantages. Its resistivity and its temperature coefficient of resistivity are higher which cause greater Joule heating of the metallization when operating at high current densities. Adherence of the metal to the substrate and wire bonding can also create problems.